Article

SOURCE DATA TRANSPARENT PROCESS

THE EMBO JOURNAL

Cytosolic GDH1 degradation restricts protein synthesis to sustain tumor cell survival following amino acid deprivation

Jialiang Shao[1,*], Tiezhu Shi[1], Hua Yu[2,3], Yufeng Ding[1], Liping Li[3], Xiang Wang[1] & Xiongjun Wang[2,3,**]

Abstract

The mTORC1 pathway plays key roles in regulating various biological processes, including sensing amino acid deprivation and driving expression of ribosomal protein (RP)-coding genes. In this study, we observed that depletion of glutamate dehydrogenase 1 (GDH1), an enzyme that converts glutamate to α-ketoglutarate (αKG), confers resistance to amino acid deprivation on kidney renal clear cell carcinoma (KIRC) cells. Mechanistically, under conditions of adequate nutrition, GDH1 maintains RP gene expression in a manner dependent on its enzymatic activity. Following amino acid deprivation or mTORC1 inhibition, GDH1 translocates from mitochondria to the cytoplasm, where it becomes ubiquitinated and degraded via the E3 ligase RNF213. GDH1 degradation reduces intracellular αKG levels by more than half and decreases the activity of αKG-dependent lysine demethylases (KDMs). Reduced KDM activity in turn leads to increased histone H3 lysine 9 and 27 methylation, further suppressing RP gene expression and preserving nutrition to support cell survival. In summary, our study exemplifies an economical and efficient strategy of solid tumor cells for coping with amino acid deficiency, which might in the future be targeted to block renal carcinoma progression.

Keywords amino acid deprivation; GDH1; kidney cancer; ribosomes; αKG
Subject Categories Cancer; Chromatin, Transcription & Genomics; Metabolism
DOI 10.15252/embj.2020107480 | Received 9 December 2020 | Revised 4 June 2021 | Accepted 13 June 2021 | Published online 16 July 2021
The EMBO Journal (2021) 40: e107480

Introduction

Solid tumors frequently undergo nutrient limitation, such as amino acid (aa) or glucose deprivation, during rapid progression without matching angiogenesis. Autophagy and increased uptake of nutrients are well-established strategies for tumor cells to cope with nutrient limitation. Autophagy is a process in which tumors actively or inactively sacrifice some cells and release glucose, aa, or lipids, which are utilized by the remaining tumor cells. Autophagy requires the consumption of precious energy, including ATP, and induces an imbalance in the NADH/NADPH pool (Rabinowitz & White, 2010; Bento *et al*, 2016). More importantly, as autophagy is a long-term selection of tumor cells for metabolic reprogramming, how tumor cells rapidly respond following aa starvation is largely unknown. mTORC1, also known as mammalian target of rapamycin complex 1 or mechanistic target of rapamycin complex 1, functions as a nutrient/energy/redox sensor and controls protein synthesis (Saxton & Sabatini, 2017). As mTORC1 senses the abundance of amino acids in the microenvironment, mTORC1 is inactivated when aa deprivation occurs or Torin 1 efficiently inhibits mTORC1 activity (Ben-Sahra & Manning, 2017; Rabanal-Ruiz *et al*, 2017).

Glutamate dehydrogenase 1 (GDH1), an important enzyme of glutaminolysis, produces αKG through its glutamate dehydrogenation activity. In addition to its metabolic roles, αKG also functions as a cofactor of DNA dioxygenases, such as KDMs and TETs (DeLuna *et al*, 2001; Rose *et al*, 2011; Legendre *et al*, 2020). αKG is produced by GDH1/2, IDH1/2, GOT1/2, and GPT and depleted by OGDH, PSAT1, and BCAT1/2 (Islam *et al*, 2018). Alterations in the intracellular level of αKG could regulate the expression of various genes. In the present study, we observed a decrease in the intracellular αKG level by more than half in KIRC cells after GDH1 depletion, suggesting that GDH1 produced the majority of αKG in KIRC cells. Additionally, the expression levels of 49 of approximately 80 RP genes were significantly downregulated by GDH1 depletion.

Ribosome biogenesis is critical for cells to generate the ribosomes needed for protein synthesis, which is a complex process involving the coordinated production of four different RNA species and approximately 80 RPs, as well as their assembly into functional ribosomal subunits (Chaillou *et al*, 2014; Catez *et al*, 2019). mTORC1 plays a key role in positively regulating ribosome biogenesis, including ribosomal RNA transcription and the synthesis of ribosomal proteins and other components required for ribosome assembly (Ma & Blenis, 2009; Iadevaia *et al*, 2014). Although critical advances

1 Department of Urology, Shanghai General Hospital, Shanghai Jiao Tong University, Shanghai, China
2 CAS Key Laboratory of Tissue Microenvironment and Tumor, Institute of Nutrition and Health Sciences, Chinese Academy of Sciences, University of Chinese Academy of Sciences, Shanghai, China
3 School of Life Sciences, Guangzhou University, Guangzhou, China
*Corresponding author. Tel: +86 13818488610; E-mail: alexshaojialiang@126.com
**Corresponding author. Tel: +86 13764412985; E-mail: wangxiongjun@gzhu.edu.cn or xiongjunwang@sibs.ac.cn

© 2021 The Authors

have been made in understanding mTORC1 signaling, the comprehensive molecular mechanisms by which mTORC1 regulates ribosome biogenesis remain unclear. A previous study showed that inhibition of mTORC1 or its downstream kinase S6K1 impaired RP gene expression, but how mTORC1 signaling cascades transduce and mediates RP gene expression is not well known.

Given the high demand for amino acids and nucleotides in ribosome biogenesis, the latter is also a metabolically expensive process for the cell. GDH1 is mainly localized in the mitochondria; however, following aa deprivation, GDH1 translocates from the mitochondria to the cytoplasm. Mitochondrial-cytoplasm translocation is accompanied by GDH1 degradation. Furthermore, we found that the E3 ligase RNF213 associates with GDH1 in the cytoplasm and guides the degradation of cytoplasmic GDH1, which induces a reduction in the intracellular αKG level and supports KIRC cell survival.

αKG-dependent dioxygenases, such as EGLNs or TETs, display differences in their binding affinity to αKG. The *Km* values of αKG for EGLNs and TETs vary from 1 to 10 μM (Xiao *et al*, 2012; Lorenzo *et al*, 2014), while those of αKG for KDMs are approximately 25–100 μM, indicating that a decreased cellular level of αKG would first affect KDM activity (Xu *et al*, 2011; Mullen *et al*, 2014). KDMs control H3 methylation and target various genes (Berry & Janknecht, 2013; Shpargel *et al*, 2014; Carrer & Wellen, 2015). For example, a loss of PHGDH induces increased H3K27me3, which is demethylated by KDM6A/6B (Baksh *et al*, 2020). In the present study, we observed that KDMs, particularly KDM4A and KDM6A, occupied the promoter of RP genes in KIRC cells and coordinately shut down RP gene expression following amino acid deprivation.

We conclude that the RNF213/GDH1/KDMs axis adapts KIRCs from a proliferating state to survive following nutrient limitation and offers a therapeutic strategy for cancer treatment. In this axis, αKG works as the key transducer, and delivering permeable αKG could efficiently inhibit tumor progression by inducing uncontrolled protein synthesis, which further exhausts energy sources under nutrient limitation.

Results

GDH1 promotes protein synthesis by fueling ribosomal protein-coding gene expression and is inversely correlated with the prognosis of KIRC patients

Protein synthesis is essential for cell growth but is not suitable during cell survival under nutrient limitation. To discover the role of GDH1 in aa deprivation, we constructed the cells stably knocking down GDH1 and found that GDH1 depletion reduced the intracellular αKG level for a range of 60% to 70%, suggesting that GDH1 is the major metabolic enzyme for αKG production in KIRC cells (Fig EV1A and B). We observed an increased tolerance of tumor cells to aa deprivation following GDH1 depletion in KIRC cells (Figs 1A and EV1C). To exclude the possibility of off-target effects, we reintroduced different doses of GDH1 into cells lacking GDH1 (Fig EV8D), and forced expression of GDH1 at a dose of three times elevated the intracellular αKG level by approximately 100% (Fig EV1E). As shown in Fig. 1B, with increased GDH1 expression, the sensitivity of KIRC cells to aa deprivation increased (Figs 1B and EV1F). To clarify how GDH1 exerts its effect on KIRC cells and sensitizes cells to aa deprivation, we performed RNA sequencing and GO cellular component and KEGG pathway enrichment analyses. The transcription of ribosomal protein genes was significantly affected among cellular components and KEGG pathways (Fig 1C and D). Gene set enrichment analysis (GSEA) and a heatmap showed declines in RP genes with the loss of GDH1 (Fig 1E and F). We also confirmed the top 10 RP genes most likely regulated by GDH1 using qPCR (Fig EV1G and H).

Therefore, we speculate that GDH1 promotes protein synthesis by maintaining RP gene expression. To confirm this speculation, we used a protein synthesis assay kit, which is a non-radioactive method for measuring protein synthesis that employs the cell-permeable, alkyne-containing, puromycin analog O-propargyl-puromycin (OPP; Rosenblum *et al*, 2012). Coomassie Brilliant Blue

Figure 1. GDH1 promotes protein synthesis by maintaining ribosomal protein (RP) expression and inversely correlates with the CRC patient prognosis.

A 786-0 or 769-P cells stably expressing shNT or shGDH1 were treated with or without aa starvation for the indicated times, and then, cell viability was assessed.

B 786-0 or 769-P cells stably expressing shNT or shGDH1 were reconstituted with or without various amounts of rGDH1-WT (3*WT indicates 3-fold expression WT) and then treated with aa starvation for the indicated time. Cell viability was subsequently assessed.

C–E RNA-Seq analyses were performed in 786-0 cells stably expressing shNT or shGDH1 treated with or without aa starvation for 12 h. Gene ontology cellular components (C) and KEGG enrichment (D) analysis of differentially expressed genes were performed using shNT- and shGDH1-expressing 786-0 cells. The enrichment of differentially expressed ribosomal protein-coding genes was measured by GSEA (E).

F Heatmap of all of the ribosomal protein-coding genes in shNT and shGDH1 cells.

G Coomassie Brilliant Blue (CBB) staining and protein synthesis assays using the Cayman kit (601100) were performed in cells with or without GDH1. Western blotting (WB) was performed with the indicated antibodies. β-Actin was used as a loading control (left). The Click-iT HPG kit (C10428) is also used to detect newly synthesized proteins in cells with or without GDH1 (right).

H Boxplots of GDH1 expression between primary CRC tumors and adjacent normal tissues in the TCGA-KIRC cohort. In the boxplot, medians, 0.25/0.75 quantile, and min/max were represented by the central lines, the box limits, and the whiskers, respectively (N: normal, $n = 72$; T: tumor, $n = 534$). Unpaired *t*-test was used with $^{***}P < 0.001$.

I IHC staining of GDH1 in primary KIRC tumors and adjacent normal tissues collected by us was performed (left). Quantitative analysis of the GDH1 protein levels was performed using unpaired *t*-test (right). $^{***}P < 0.001$. Scale bars: 50 μm.

J Boxplots of GDH1 expression in four stages in the TCGA-KIRC cohort. In the boxplot, medians, 0.25/0.75 quantile, and min/max were represented by the central lines, the box limits, and the whiskers, respectively (I: $n = 267$, II: $n = 57$, III: $n = 123$, IV: $n = 84$). One-way ANOVA test was used with $^{**}P < 0.01$.

K Overall survival of patients in different tumor stages in the TCGA-KIRC cohort. The R package "survminer"-based maximally selected log-rank statistic was used to determine the best cutoff. The log-rank test was used to determine the *P*-value.

Data information: (A, B and G) The data are represented as means ± SEM of three independent experiments, and all statistical analyses were conducted using unpaired *t*-test ($^{**}P < 0.01$; $^{***}P < 0.001$). See also Fig EV1.
Source data are available online for this figure.

 © 2021 The Authors

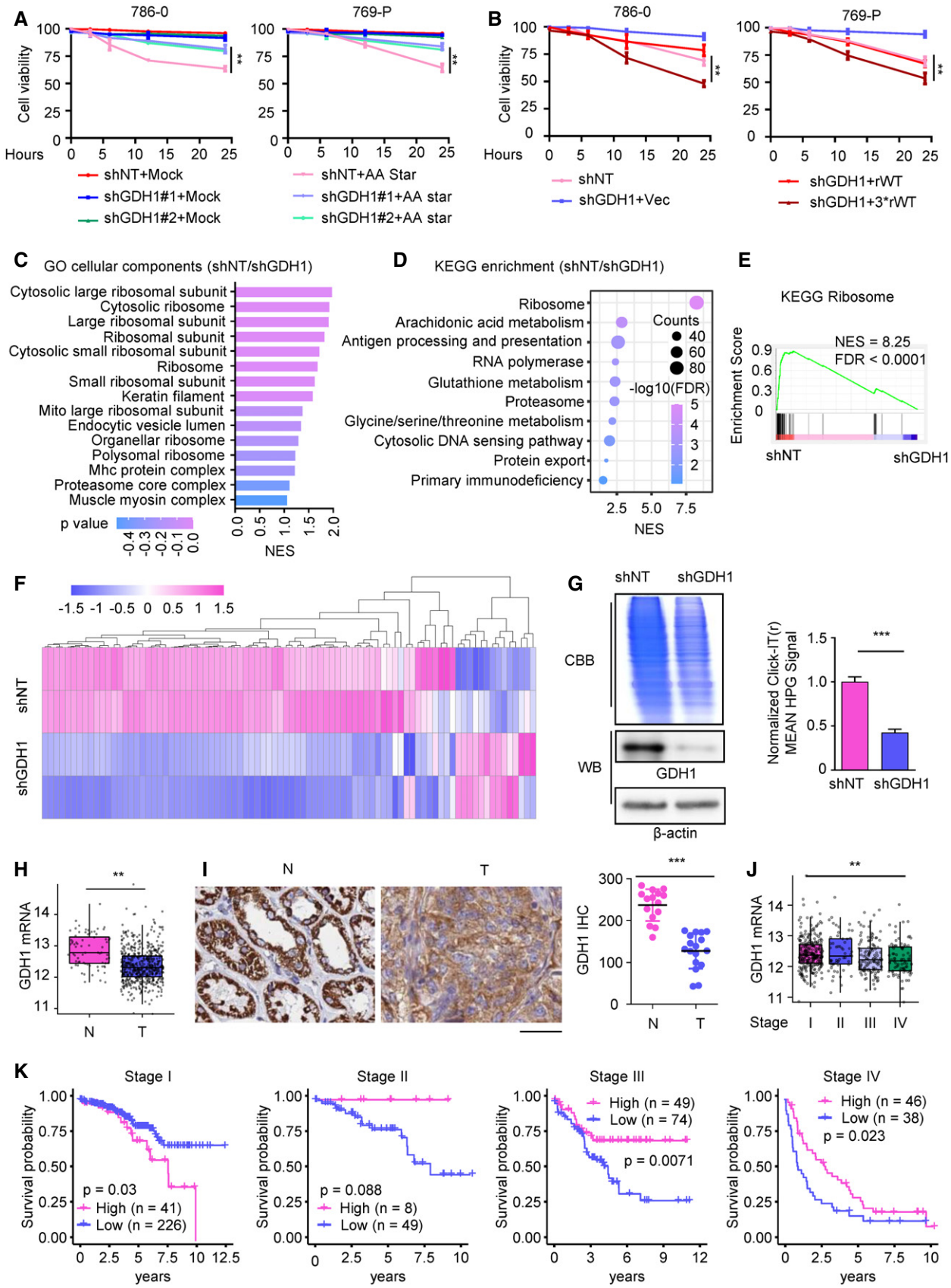
A
786-0
769-P
Cell viability
Hours
shNT+Mock
shGDH1#1+Mock
shGDH1#2+Mock
shNT+AA Star
shGDH1#1+AA star
shGDH1#2+AA star
B
786-0
769-P
Cell viability
Hours
shNT
shGDH1+Vec
shGDH1+rWT
shGDH1+3*rWT
C
GO cellular components (shNT/shGDH1)
Cytosolic large ribosomal subunit
Cytosolic ribosome
Large ribosomal subunit
Ribosomal subunit
Cytosolic small ribosomal subunit
Ribosome
Small ribosomal subunit
Keratin filament
Mito large ribosomal subunit
Endocytic vesicle lumen
Organellar ribosome
Polysomal ribosome
Mhc protein complex
Proteasome core complex
Muscle myosin complex
p value
NES
D
KEGG enrichment (shNT/shGDH1)
Ribosome
Arachidonic acid metabolism
Antigen processing and presentation
RNA polymerase
Glutathione metabolism
Proteasome
Glycine/serine/threonine metabolism
Cytosolic DNA sensing pathway
Protein export
Primary immunodeficiency
Counts
-log10(FDR)
NES
E
KEGG Ribosome
NES = 8.25
FDR < 0.0001
Enrichment Score
shNT
shGDH1
F
shNT
shGDH1
G
shNT
shGDH1
CBB
WB
GDH1
β-actin
Normalized Click-IT(r) MEAN HPG Signal
H
GDH1 mRNA
N
T
I
N
T
GDH1 IHC
J
GDH1 mRNA
Stage
K
Stage I
Stage II
Stage III
Stage IV
Survival probability
p = 0.03
High (n = 41)
Low (n = 226)
p = 0.088
High (n = 8)
Low (n = 49)
High (n = 49)
Low (n = 74)
p = 0.0071
High (n = 46)
Low (n = 38)
p = 0.023
years

Figure 1.

(CBB) staining, the BCA assay, and a protein synthesis kit demonstrated that the loss of GDH1 impaired protein synthesis (Figs 1G and EV1I). Cell line-based experiments proved that the high expression of GDH1 was not conducive to the survival of renal cancer cells in adverse nutritional environments, such as amino acid deficiency. We next mined GDH1 expression in the TCGA database and confirmed the database results using our own collected samples. GDH1 was downregulated in KIRC tissues, particularly at the protein level, indicating that the decreased expression of GDH1 would facilitate renal cancer initiation (Fig 1H and I). The ability of tumor cells to stress the vegetative microenvironment is closely related to tumor treatment and patient survival. With the increase in tumor grade, the mRNA and protein levels of GDH1 decreased (Fig 1J). Notably, survival analysis of patients with different tumor stages from the TCGA-KIRC cohort showed that patients with lower GDH1 expression survived better in early-stage I, indicating that GDH1 plays an aggressive role in low-grade renal carcinoma, which has an abundant supply of nutrients for GDH1-mediated protein synthesis. However, as the tumor progressed, patients with low GDH1 expression had a poor prognosis, probably because high GDH1 expression in the late stage of the tumor impaired the progression of renal cell carcinoma, suggesting that GDH1 is a potential tumor suppressor of advanced renal cell carcinoma (Fig 1K). The von Hippel-Lindau (VHL) mutation frequently occurs in KIRC. However, GDH1 expression was not associated with the VHL mutation (Fig EV1J and K). All of the above clinical indications suggest that high expression of GDH1 is not conducive to KIRC progression.

The deprivation of aa induces GDH1 translocation and reduces protein stability

As a high level of GDH1 sensitizes KIRC cells to aa deprivation, we wanted to further investigate the KIRC response to aa deprivation using GDH1. We collected KIRC cells over a time course of aa deprivation treatment and observed a continuous decrease at the GDH1 protein level but not at the mRNA level (Fig 2A and B). A more rigorous experiment confirmed that aa deprivation significantly decreased the protein stability of GDH1 compared with that of the control group without aa deprivation (Fig 2C). GDH1 is mainly localized in the mitochondria; surprisingly, aa deprivation induced GDH1 diffusion into the cytoplasm (Fig 2D and E). The mTORC1 complex senses amino acid abundance, and amino acid deprivation inactivates mTORC1. To mimic the inactivation of mTORC1 by aa deprivation, we applied an inhibitor of mTORC1, Torin 1 (Ben-Sahra & Manning, 2017). When we treated KIRC cells with Torin 1, GDH1 was forced out of the mitochondria and entered the cytoplasm (Fig EV2A and B). Tuberous sclerosis complex (TSC) negatively regulates mTOR signaling activation (Saxton & Sabatini, 2017), and knockout of the *TSC1* gene in 786-0 cells showed the mitochondrial localization of GDH1 with or without aa starvation (Fig EV2C). *TSC1*$^{-/-}$ cells were hypersensitive to aa deprivation (Fig EV2D). Ribosomal S6 kinase (S6K) works as an adaptor and a substrate of mTORC1, and its activity controls the ribosome biogenesis transcriptional program (Chauvin *et al*, 2014). A specific inhibitor of S6K, LY2584702, was used to treat 786-0 cells, and we observed the cytosolic localization of GDH1 with or without aa starvation (Fig EV2E). Thus, the activation of the mTOR-S6K pathway is required for maintaining the distribution ratio of GDH1 under abundant or scarce aa. More importantly, this translocation from the mitochondria to the cytoplasm could be associated with the reduction in GDH1 protein level (Fig 2F). The N-terminus of the GDH1 protein comprises a mitochondrial signal peptide (MSP; Plaitakis *et al*, 2000; Kotzamani & Plaitakis, 2012). When we deleted this MSP, GDH1 did not enter the mitochondria and was localized in the cytoplasm with a reduced protein level but was not impaired at the mRNA level (Figs 2G and H and Fig EV2F and G). As expected, preventing GDH1 from entering the mitochondria was also associated with reduced GDH1 protein stability, at a similar level to that of aa starvation stress (Fig 2I). We observed that GDH1 degrades rapidly when the cells receive the aa starvation stimulus after blocking fresh protein synthesis (Fig EV2I). Hence, we speculate that localization in the mitochondria or cytoplasm determines GDH1 protein stability.

Figure 2. The starvation of aa induces GDH1 translocation and reduces protein stability.

A 786-0 cells were subjected to aa starvation for the indicated times. The protein level of GDH1 was determined by WB using the indicated antibody.
B The mRNA level of GDH1 in the cells in (A) was determined by qPCR using specific primers against GDH1 mRNA.
C 786-0 cells were treated with or without aa starvation for 6 h and then treated with CHX (1 μM) for the indicated times. The protein level of GDH1 was determined by Western blotting (left), and the relative GDH1 protein levels were calculated (right). CHX: cycloheximide. Unpaired *t*-test was used.
D Immunofluorescence (IF) assay was performed to determine the subcellular location of GDH1 with or without aa starvation. GDH1 localization was indicated by GDH1 antibody and MitoTracker (left). Signal intensities and distances were quantified (right). Scale bars: 20 μm.
E Cytoplasm-mitochondrial fractionation assay was performed to determine the subcellular location of GDH1 with or without aa starvation. The fractionation efficiency and GDH1 location were determined by WB using antibodies against VDAC1 (mitochondrial membrane marker) and GDH1. Tubulin was used as loading control.
F The total GDH1 protein in 786-0 and 769-P cells with or without aa starvation for 12 h was measured by WB.
G Immunofluorescence (IF) assay was performed to determine the subcellular location of WT or mitochondrial signal peptide deleted (dMSP) GDH1. GDH1 localization was indicated by GDH1 antibody and MitoTracker (left). Signal intensities and distances were quantified (right). Scale bars: 20 μm.
H Cytoplasm-mitochondrial fractionation assay was performed to determine the subcellular location of WT or mitochondrial signal peptide deleted (dMSP) GDH1. The fractionation efficiency and GDH1 location were determined by WB using antibodies against VDAC1 (mitochondrial membrane marker) and GDH1. Tubulin was used as loading control.
I 786-0 cells with FLAG-tagged WT or dMSP GDH1 were treated with CHX (1 μM) for the indicated times. The protein level of FLAG-tagged WT or dMSP GDH1 was determined by Western blotting (left). The relative WT or dMSP GDH1 protein level was calculated (right). Unpaired two-tailed *t*-test was used.

Data information: (B, C and I) The data are represented as mean ± SEM of three independent experiments. The one-way ANOVA test (B) and unpaired *t*-test were used (C and I). (N.S.: not significant; ***$P < 0.001$). See also Fig EV2.
Source data are available online for this figure.

 © 2021 The Authors

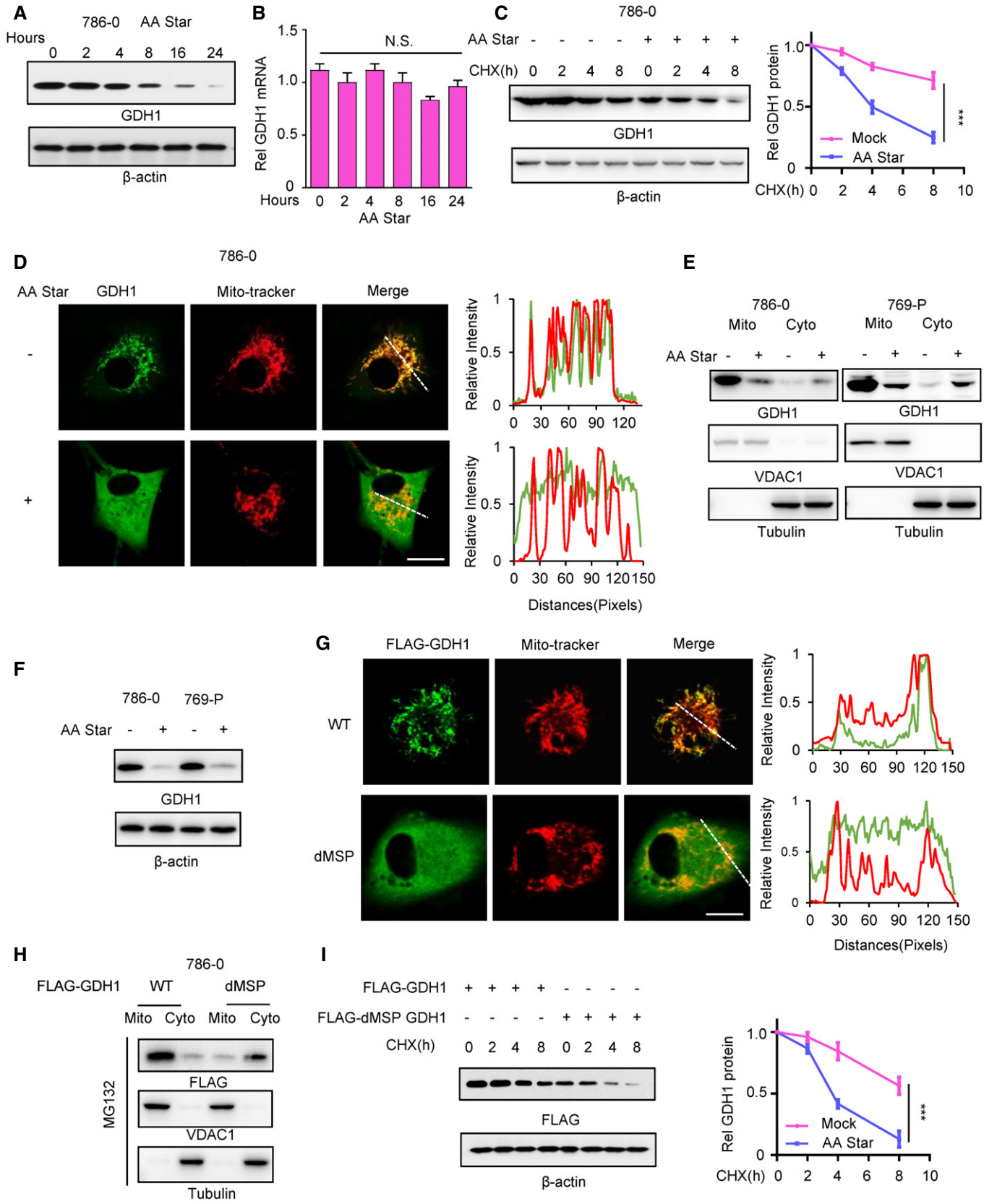
A
786-0 AA Star
Hours 0 2 4 8 16 24
GDH1
β-actin
B
N.S.
Rel GDH1 mRNA
1.5
1.0
0.5
0
Hours 0 2 4 8 16 24
AA Star
C
786-0
AA Star - - - - + + + +
CHX(h) 0 2 4 8 0 2 4 8
GDH1
β-actin
Rel GDH1 protein
1.0
0.5
0
Mock
AA Star
***
CHX(h) 0 2 4 6 8 10
D
786-0
AA Star GDH1 Mito-tracker Merge
-
+
Relative Intensity
1
0.5
0
0 30 60 90 120
0 30 60 90 120 150
Distances(Pixels)
E
786-0 769-P
Mito Cyto Mito Cyto
AA Star - + - + - + - +
GDH1
VDAC1
Tubulin
F
786-0 769-P
AA Star - + - +
GDH1
β-actin
G
FLAG-GDH1 Mito-tracker Merge
WT
dMSP
Relative Intensity
1
0.5
0
0 30 60 90 120 150
Distances(Pixels)
H
786-0
FLAG-GDH1 WT dMSP
Mito Cyto Mito Cyto
MG132
FLAG
VDAC1
Tubulin
I
FLAG-GDH1 + + + + - - - -
FLAG-dMSP GDH1 - - - - + + + +
CHX(h) 0 2 4 8 0 2 4 8
FLAG
β-actin
Rel GDH1 protein
1.0
0.5
0
Mock
AA Star
***
CHX(h) 0 2 4 6 8 10

Figure 2.

Ubiquitination of a cluster of lysines impairs GDH1 protein stability under aa deprivation

Presently, there are two major degradation pathways—the lysosome degradation pathway and ubiquitin-dependent proteasome degradation pathway—which are inhibited by chloroquine (CQ) and MG132, respectively (Goold *et al*, 2015; Clausen *et al*, 2019). In the present study, MG132 treatment rescued the GDH1 protein level under aa deprivation, while CQ did not affect the GDH1 protein level in KIRC cells (Fig 3A). After co-transfecting HA-tagged ubiquitin with Flag-tagged GDH1, we observed that aa deprivation induced increased ubiquitin modifications in GDH1 (Fig 3B). We further clarified that aa starvation-induced instability of GDH1 is regulated by the type of K48 ubiquitination (Fig EV3A). LC-MS/MS identified a total of 13 ubiquitinated lysine when KIRC cells were treated with or without aa deprivation. We displayed this result using a heatmap, which showed that GDH1-K183, GDH1-K191, and GDH1-K200 had enhanced ubiquitin modification after aa deprivation (Fig 3C). To verify which lysine residues among K183, K191, and K200 contribute to GDH1 protein stability, we mutated these three lysine residues to arginines as indicated in Fig 3D. However, each mutation of lysine to arginine at GDH1-K183, GDH1-K191, or GDH1-K200 equally increased GDH1 protein stability. As the number of mutated sites increased, the protein stability of GDH1 also increased. Mutating K183, 191, and 200 to R183, 191, and 200 (3KR) completely reduced the increased ubiquitin modifications induced by aa deprivation (Fig 3E). Successful construction of the 3KR mutant showed that the 3KR mutant promoted GDH1 stability under aa starvation (Fig EV3B and C) but had the same enzymatic activity as wild-type GDH1 (Fig 3F). We also excluded the possibility that the enzyme dead and 3KR mutant affect GDH1 localization with or without aa deprivation (Fig EV3D). Thus, the ubiquitination of the lysine cluster of K183, 191, and 200 facilitates GDH1 degradation under aa limitation without affecting its own enzymatic activity. Consequently, the increased GDH1 protein upregulates RP gene expression and sensitizes KIRCs to aa deprivation (Fig 3G and H), and inhibition of GDH1-mediated protein synthesis facilitates cell survival under aa deprivation (Fig EV3E and F). Therefore, we initially linked the localization of GDH1 to its stability and the expression of RP genes.

RNF213 is required for GDH1 ubiquitin under aa deprivation

To screen which E3 ligase is required for inducing the degradation of GDH1, we first knocked GFP into the GDH1 C-terminus (Fig EV4A). When aa deprivation stress stimulated KIRC cells, GDH1 was degraded by more than half in 8 h. The siRNAs separately target 315 E3 ligase coding genes with three siRNAs to one gene. After two rounds of independent screening, we found that three E3 ligases might be responsible for degrading GDH1 under conditions of aa deficiency (Fig 4A). Knockdown of RNF213, CHFR, or TRIM27, particularly RNF213 depletion, promoted the stability of GDH1 to varying degrees (Figs 4B and EV4B). However, an endogenous co-IP assay demonstrated that GDH1 was associated more with RNF213 than CHFR or TRIM27 (Fig 4C). We suspect that the depletion of CHFR or TRIM27 increased GDH1 protein levels via an indirect connection. Reverse co-IP using an RNF213 antibody further confirmed the interaction between RNF213 and GDH1 (Fig 4D). The specificity of this interaction was demonstrated after RNF213 depletion, and a co-IP assay was performed using an antibody against GDH1 or RNF213 (Figs 4E and EV4C).

An *in vitro* ubiquitination assay identified that RNF213 ubiquitinated GDH1 at K183, 191, and 200 (Fig EV4D). RNF213 depletion specifically increased GDH1 ubiquitination at K183, 191, and 200 under aa starvation, leading to stabilized GDH1 protein (Fig 4F and G) and finally increased RP gene expression (Fig EV4E). Consistently, we observed that RNF213 depletion sensitized KIRC cells to aa deprivation, and this sensitivity was counteracted by GDH1 depletion. Additionally, we demonstrated that KIRC cells were impaired by GDH1 depletion (Fig EV4F and G) and that RNF213 contributed to KIRC aa deprivation tolerance by degrading GDH1 (Fig 4H). The reverse association between the protein levels of GDH1 and RNF213 was further demonstrated in clinical KIRC samples, and high RNF213 expression was positively correlated

Figure 3. Ubiquitination of a cluster of lysines impairs GDH1 protein stability under aa starvation.

A 786-0 or 769-P cells were pretreated with or without aa starvation for 6 h, and then, MG132 (10 μM) or CQ (1 μM) was added to the cell culture medium for 12 h. The protein level of GDH1 was determined by WB with the indicated antibody.

B In 786-0 cells, FLAG-tagged GDH1 was co-transfected with or without HA-tagged ubiquitin for 48 h, and then, the cells were treated with or without aa starvation for 6 h. Immunoprecipitation was performed using an antibody against FLAG followed by Western blotting using the indicated antibodies.

C In 786-0 cells, FLAG-tagged GDH1 was co-transfected with HA-tagged ubiquitin for 48 h, and then, the cells were treated with or without aa starvation for 6 h. Immunoprecipitation (IP) was performed using an antibody against FLAG, and the ubiquitination of FLAG-GDH1 was identified by LC-MS/MS.

D FLAG-tagged GDH1 (including WT and mutants with different lysine mutations to arginine) was co-transfected with HA-tagged ubiquitin for 48 h, and then, cells were subjected to aa starvation for 12 h before collecting cells. WB and qPCR separately tested the levels of GDH1 protein and mRNA, respectively.

E FLAG-tagged GDH1 (including WT and 3KR mutant) and HA-tagged ubiquitin-expressing 786-0 cells were pretreated with aa starvation for 12 h before treatment with MG132 (10 μM) for 12 h. Immunoprecipitation was performed using an antibody against FLAG followed by WB using the indicated antibodies. 3KR mutant: lysine 183, 191, 200 to arginine 183, 191, 200.

F FLAG-tagged GDH1 (including WT and 3KR mutant) was transfected into HEK293T cells and enriched using an antibody against FLAG. GDH1 enzymatic activity was quantified, and the quantity of WT and 3KR GDH1 was evaluated by CBB staining. Unpaired two-tailed *t*-test was used.

G Restored expression of wild-type or 3KR mutant in 786-0 cells lacking GDH1 followed by pretreatment of the cells with or without aa starvation for 24 h. Cells were collected, and total RNA was extracted for further qPCR using primers against the mRNA of RP genes.

H 786-0 or 769-P cells stably expressing shGDH1 were reconstituted with rGDH1-WT or 3KR mutant and then treated with or without aa starvation for the indicated time. Cell viability was determined. Unpaired two-tailed *t*-test was used.

Data information: (D, F and H) The data are represented as the mean ± SEM of three independent experiments. The one-way ANOVA test (D) and unpaired *t*-test were used (F and H). (N.S.: not significant; *$P < 0.05$; **$P < 0.01$; ***$P < 0.001$). See also Fig EV3.
Source data are available online for this figure.

 © 2021 The Authors

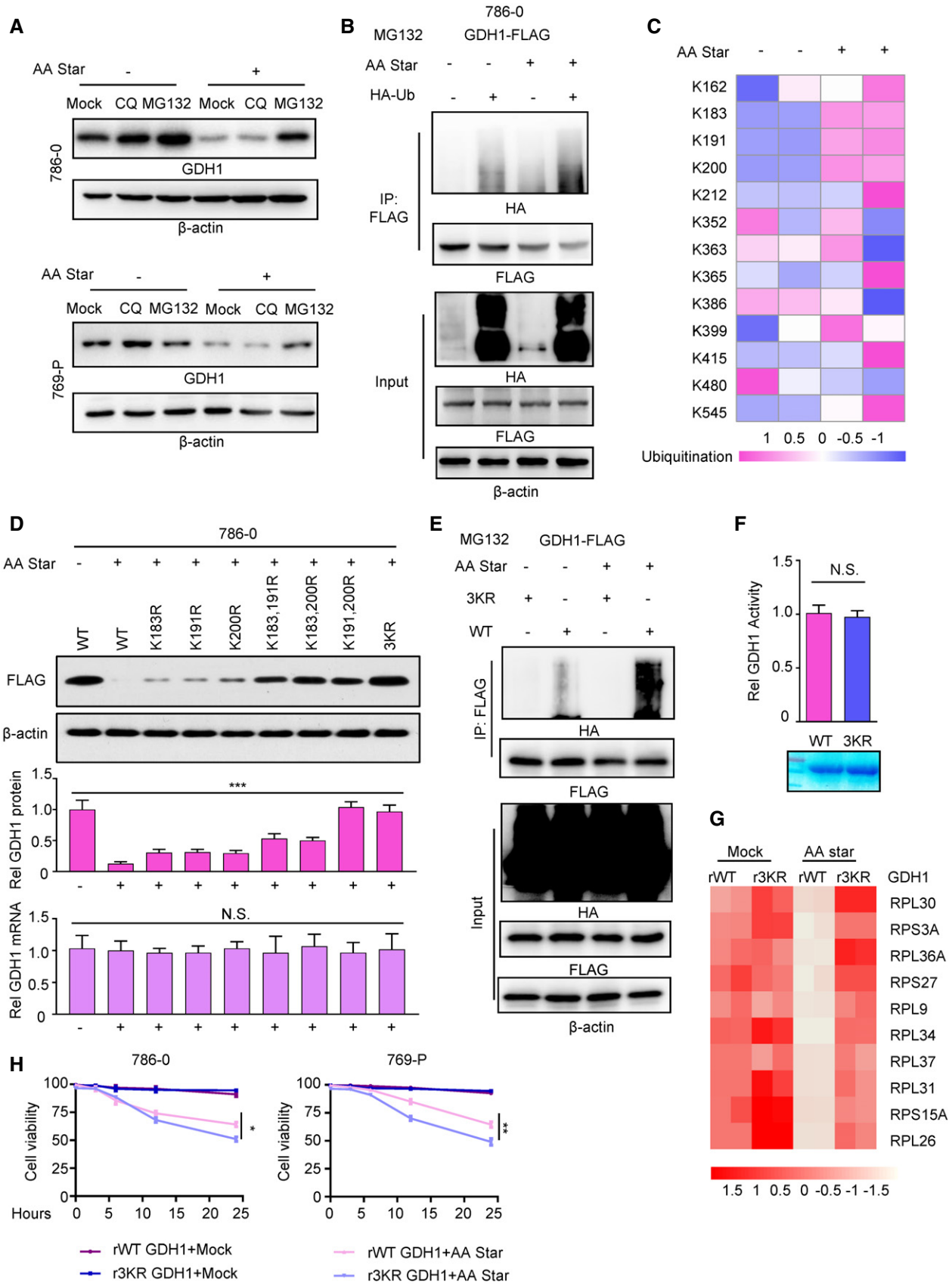
A
AA Star - +
Mock CQ MG132 Mock CQ MG132
786-0
GDH1
β-actin
AA Star - +
Mock CQ MG132 Mock CQ MG132
769-P
GDH1
β-actin
B
786-0
MG132 GDH1-FLAG
AA Star - - + +
HA-Ub - + - +
IP: FLAG
HA
FLAG
Input
HA
FLAG
β-actin
C
AA Star - - + +
K162
K183
K191
K200
K212
K352
K363
K365
K386
K399
K415
K480
K545
1 0.5 0 -0.5 -1
Ubiquitination
D
786-0
AA Star - + + + + + + + +
WT WT K183R K191R K200R K183,191R K183,200R K191,200R 3KR
FLAG
β-actin
Rel GDH1 protein
***
Rel GDH1 mRNA
N.S.
E
MG132 GDH1-FLAG
AA Star - - + +
3KR + - + -
WT - + - +
IP: FLAG
HA
FLAG
Input
HA
FLAG
β-actin
F
Rel GDH1 Activity
N.S.
WT 3KR
G
Mock AA star
rWT r3KR rWT r3KR GDH1
RPL30
RPS3A
RPL36A
RPS27
RPL9
RPL34
RPL37
RPL31
RPS15A
RPL26
1.5 1 0.5 0 -0.5 -1 -1.5
H
786-0
769-P
Cell viability
Hours
rWT GDH1+Mock
r3KR GDH1+Mock
rWT GDH1+AA Star
r3KR GDH1+AA Star

Figure 3.

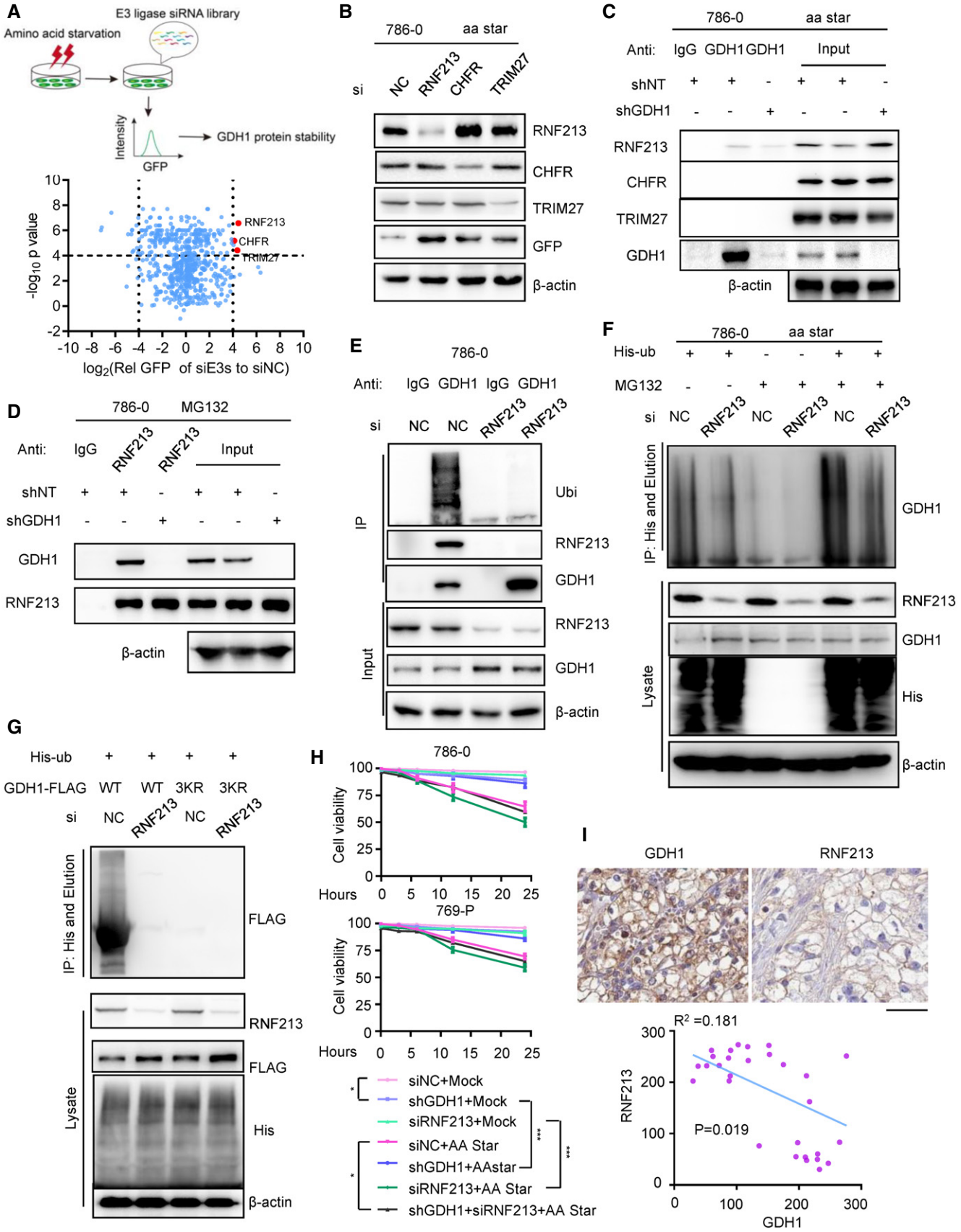

Figure 4.

© 2021 The Authors

Figure 4. RNF213 is required for GDH1 ubiquitination under aa starvation.

A 786-0 cells were transfected with individual siRNAs that targeted 335 E3 ligases (three siRNAs per gene; indicated as "siGene" on the x-axis) for 48 h and treated with aa starvation for 12 h in duplicates. Next, the intensity of GDH1-GFP in each well was recorded using Opera Phenix (Perkin Elmer). The data are presented as a volcano plot. The siRNAs with $P < 0.0001$ (two-tailed Student's *t*-test) and a GFP intensity ratio (normalized to the non-targeting siRNA) > 16 were considered to be effective siRNAs (red). E3 ligases targeted by more than two effective siRNAs were selected as candidates. siE3s, E3 ligase siRNAs; siNC, non-targeting control siRNA.

B 786-0 cells were transfected with siRNA targeting RNF213, CHFR, or TRIM27 for 48 h and then were subjected to aa starvation for 12 h. WB was performed using the indicated antibodies.

C, D 786-0 cells were treated with MG132 (10 μM) under aa starvation. Antibodies against GDH1 (C) or RNF213 (D) were used to enrich protein complexes in cells with or without GDH1. IgG was used as a control. WB was performed using the indicated antibodies.

E 786-0 cells were treated with MG132 (10 μM) under aa starvation. The cells were transfected with siNC or siRNF213 for 48 h, and then, an antibody against GDH1 was used to enrich the GDH1-associated complex. IgG was used as a control. WB was performed using the indicated antibodies.

F 786-0 cells were transfected with siNC or siRNF213 for 24 h and then were transfected with or without His-ubiquitin for 36 h. The indicated cells were treated with or without MG132 (10 μM) under aa starvation. Beads against His were used to enrich His-ubiquitin-associated proteins, which were eluted by PBS containing 250 mM imidazole. WB was performed using the indicated antibodies.

G Restored expression of WT or 3KR GDH1 in 786-0 cells lacking GDH1 followed by transfection with or without His-ubiquitin for 36 h. The indicated cells were treated with MG132 (10 μM) under aa starvation. Beads against His were used to enrich His-ubiquitin-associated proteins in the indicated cells. WB was performed using the indicated antibodies.

H 786-0 or 769-P cells (WT or stably expressing shGDH1) were transfected with siNC or siRNF213 for 48 h and then were treated with or without aa starvation for the indicated times. Cell viability was determined. Unpaired *t*-test was used with ***$P < 0.001$.

I IHCs of KIRC clinical samples were performed using antibodies against GDH1 or RNF213 (upper panel). The correlated IHC signal between GDH1 and RNF213 in KIRC samples was calculated (lower panel). The cor.test was used to determine the *P*-value. Scale bars: 50 μm.

Source data are available online for this figure.

with a poor patient prognosis (Figs 4I and EV4H). These data demonstrate that RNF213 is required for GDH1 ubiquitination under aa deprivation and is inversely correlated with the GDH1 protein level in cell lines and clinical KIRC tissue.

Increased cellular αKG sensitizes tumor cells to aa deprivation

The deprivation of aa induces GDH1 degradation, and GDH1 depletion leads to a decrease in αKG by more than 60% in KIRC cells (Fig V1C). Notably, the enzyme-dead (ED) mutant of GDH1 impaired αKG production to a similar degree as the degradation of GDH1 under aa deprivation (Fig 5A and B and Appendix Figs S1A and S2A). A similar degree of decline in αKG concentration caused by GDH1 degradation or the lack of enzyme activity induces the expression of RP genes, showing a similar decline. When we supplemented KIRC GDH1-ED cells with αKG, we observed restored expression of RP genes (Fig 5C–E), indicating that, in KIRC cells, the concentration of αKG dictates the level of RP gene expression. Downregulated RP gene expression reduced protein synthesis in KIRC cells lacking αKG (Fig 5F). As expected, the survival curve showed a similar result with GDH1 depletion in the cells lacking GDH1 enzymatic activity (Fig 5G). R-2HG (2-hydroxyglutarate), produced by mutant IDH1/2, has natural inhibitory activity against αKG (Xu *et al*, 2011). We delivered methylated 2HG into KIRC cells and found that 2HG rescued KIRC cells under aa deprivation, suggesting that competition between R-2HG and αKG exists in KIRC cells (Fig 5H and Appendix Fig S1B). A consistent result by qPCR showed that RP gene expression was also downregulated by R-2HG (Fig 5I and Appendix Fig S1C). 2HG is a tumor-suppressive or oncogenic metabolite in different cancers (DiNardo *et al*, 2013; McBrayer *et al*, 2018; Reiter-Brennan *et al*, 2018; Su *et al*, 2018). We suspected that the role of R-2HG partially depends on αKG contributing to

Figure 5. Increased cellular αKG sensitizes tumor cells to aa starvation.

A–C 786-0 cells expressing WT or enzymatically dead (ED) GDH1 were transfected with siNC or siRNF213 for 48 h and then were treated with or without aa starvation for 12 h. Western blotting was performed using the indicated antibodies (A). The intracellular level of αKG was measured using an αKG determination kit and normalized to 786-0 cells expressing WT GDH1 transfected with siNC under normal culture conditions. Unpaired *t*-test was used (B). In the above cells in (A), qPCR was used to measure the mRNA of the indicated RP genes (C).

D, E 786-0 cells expressing WT or ED GDH1 were supplemented with or without 500 μM methylated αKG for 36 h, and then, cells were collected to extract total mRNA. The mRNA levels of the indicated RP genes were tested using qPCR (D), and WB was performed using the indicated antibodies (E).

F Protein synthesis assays using the Cayman kit and Coomassie Brilliant Blue (CBB) staining were performed in the indicated cells. WB was performed using the indicated antibodies (left), and the relative intensity of protein synthesis was quantified (right). Unpaired *t*-test was used.

G 786-0 cells expressing WT or ED GDH1 were treated with or without aa starvation for the indicated times. Cell viability was determined. Unpaired two-tailed *t*-test was used.

H, I 786-0 or 769-P cells were supplemented with methylated αKG (500 μM), 2HG (500 μM), or αKG (500 μM) + 2HG (500 μM) for 36 h under aa starvation conditions. Cell viability was determined (H), and the mRNA levels of the indicated RP genes were tested using qPCR (I).

J KIRC clinical samples were collected for αKG measurement, and we assessed overall survival (left panel) with log-rank test according to the dividing groups of high and low intracellular levels of αKG with the best separation (right panel). Unpaired *t*-test was used in the right panel with ***$P < 0.001$.

Data information: (B and F–H) The data are represented as the means ± SEM of three independent experiments (N.S.: not significant; *$P < 0.05$; **$P < 0.01$; ***$P < 0.001$). See also Appendix Fig S1.
Source data are available online for this figure.

© 2021 The Authors

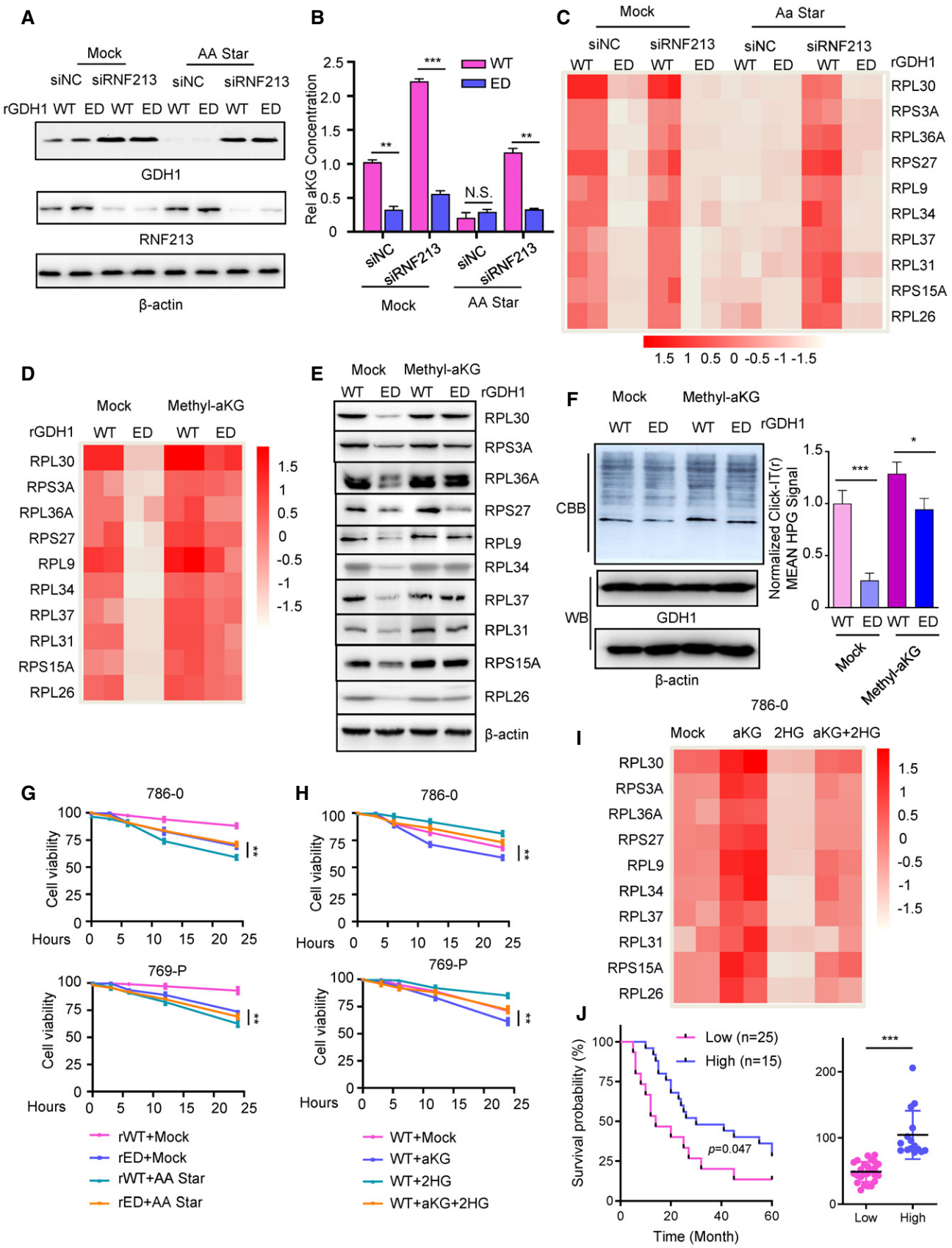

Figure 5.

© 2021 The Authors

cancers. In KIRC, a high level of αKG indicates a better prognosis for the patient (Fig 5J). So far, we have determined how αKG maintains the expression of RP genes in KIRC and that αKG does not promote the survival of tumor cells in the absence of amino acids. Therefore, using αKG to upregulate the expression of RP genes and exhaust the remnant aa of tumor cells under aa deficiency is an important strategy to inhibit KIRC progression.

KDM activity regulated by αKG is required for de-methylating H3K9me3 and H3K27me3 on the promoter of RP genes

In prokaryotic cells, all RP genes are controlled by the same operons; thus, it is convenient to coordinate the expression of RP genes following nutrient limitation (Zengel & Lindahl, 1994). Although ribosomes have an obvious relationship with protein synthesis, we still do not know how cancer cells coordinately regulate RP gene expression after sensing the abundance of amino acids in the microenvironment.

αKG epigenetically regulates gene expression by acting as a cofactor of dioxygenases, such as KDMs, which mainly contribute to demethylate the trimethylation of histone H3 (Berry & Janknecht, 2013; Shpargel *et al*, 2014; Hancock *et al*, 2015; Lamadema *et al*, 2019). We tested H3 trimethylation at lysines 4, 9, 27, and 36 in the cells with GDH1 depletion and restored the expression of WT or ED GDH1. Compared with the cells expressing rGDH1-WT, we observed reduced intracellular αKG levels (Fig 5B) and increased global levels of H3K9me3 and H3K27me3, but not H3K36me3 and H3K4me3, in the cells expressing the rGDH1-ED mutant. Supplementation with methylated αKG to cells expressing the rGDH1-ED mutant counteracted the increased global levels of H3K9me3 and H3K27me3 induced by ED GDH1 (Figs 6A and EV5A). To comprehensively understand the connection between histone H3 lysine 9, 27, and 36 trimethylation and their repressive regulation of RP genes, we performed a ChIP assay using antibodies separately against H3K9me3, H3K27me3, and H3K36me3, which targeted differentially expressed RP genes in KIRC cells with or without GDH1. The outside circle presents RP genes, while the size of the inner circle shows the intensity of H3K9me3, H3K27me3, and H3K36me3 targeting RP gene promoters with a ratio in cells containing ED and WT GDH1. Consistently, the intensity of H3K9me3 and H3K27me3 on the promoter of RP genes was displayed as the two largest groups (Fig 6B). Notably, the intensity of H3K9me3, H3K27me3, and H3K36me3 targeting the *ACTB* gene promoter was not affected (Fig EV5B). KDM4A/B/C/D and KDM6A/B contribute to the demethylation of H3K9me3 and H3K27me3 (Mosammaparast & Shi, 2010; Berry & Janknecht, 2013; Dimitrova *et al*, 2015). We performed a ChIP assay using antibodies against KDM4A/B/C/D and KDM6A/B, which likely target the RP gene promoter, and the *ACTB* gene promoter was used as a negative binding control (Fig EV5C). The circular plots present the ChIP data, showing that KDM4A and KDM6A targeted almost all of the GDH1-mediated RP genes (Fig 6C). We constructed cells lacking KDM4A or KDM6A (Fig EV5D and E) and observed that the enrichment of H3K9me3 or H3K27me3 on the promoters of RP genes increased (Figs 6D and EV5F). Additionally, the expression of these selected RP genes was downregulated in cells lacking KDM4A or KDM6A, and this downregulation was moderately rescued by excessive αKG, suggesting that excessive αKG could promote KDM demethylase activity, leading to demethylation of H3K9me3 and H3K27me3 with the overlapping of other KDM4s and KDM6s on the promoter of RP genes (Figs 6E and EV5G).

An *in vitro* demethylation assay showed that KDM4A and KDM6A displayed similar enzymatic activities of distinct H3 lysine methylation with increased αKG levels, likely because of their similar binding affinity to αKG (Figs 6F and EV5H). 2HG inhibited the binding of αKG to KDMs *in vitro*, and a level of 2HG above 50 μM efficiently blocked the enzymatic activities of KDM4A and KDM6A, most likely because the *Kd* value of KDM4A and KDM6A binding αKG was approximately 50 μM (Fig 6G). A ChIP assay further revealed that 2HG increased H3K9me3 and H3K27me3, both of which target RP gene promoters (Figs 6H and EV5I), demonstrating that 2HG negatively regulates RP gene expression by directly

Figure 6. KDM activity regulated by αKG is required to demethylate H3K9me3 and H3K27me3 on the promoter of RP genes.

A 786-0 cells expressing shGDH1 with restored expression of WT or ED GDH1 were supplemented with or without 500 μM methylated αKG for 48 h, and then, the cells were collected to extract total protein. WB was performed using the indicated antibodies.

B In 786-0 cells expressing shGDH1 with restored expression of WT or ED GDH1, the ratio (ED/WT) of H3K9me3, H3K27me3, and H3K36me3 targeting RP genes was calculated. The outer circle in the chord diagram represents the ratio of ribosomal protein-coding genes targeted by each histone lysine methylation compared with the control. The inner circles represent the sum of the indicated ratios. The IgG was used as a control.

C The relative enrichment of KDMs targeting ribosomal protein-coding genes in 786-0 cells. The outer circle represents the enrichment value of ribosomal protein-coding genes by each KDM. The inner circles represent the sum of the indicated values. The IgG was used as a control.

D 786-0 cells were transfected with siRNAs targeting KDM4A or KDM6A for 56 h, and the cells were fixed with 1% formaldehyde. ChIP assays were performed using antibodies against H3K9me3 or H3K27me3. qPCR tested the enrichment of the above histone H3 lysine modifications on the promoters of the indicated RP genes.

E 786-0 cells were transfected with siRNAs targeting KDM4A or KDM6A and then were supplemented with or without methylated αKG (500 μM) for 48 h. The cells were collected to extract total RNA, and qPCR was used to test the mRNA level of the indicated RP genes.

F Isothermal titration calorimetry (ITC) was used to test the binding affinity of αKG (1 mM) to recombinant KDM4A (0.05 mM) or KDM6A (0.05 mM) (left), and then, statistical analysis was performed (right). The data are represented as the means ± SEM of three independent experiments. Unpaired *t*-test was used (N.S.: not significant).

G An in vitro demethylation assay was performed with recombinant KDM4A (0.05 mM) or KDM6A (0.05 mM), and the indicated histone H3 lysine methylation peptides under 50-μM αKG conditions (no αKG was used as a blank control). Various concentrations of 2HG from 0 to 200 μM were used to compete with αKG in the reaction system.

H 786-0 cells were supplemented with or without 2HG (500 μM) for 48 h, and the cells were fixed with 1% formaldehyde. ChIP assays were performed using antibodies against H3K9me3 or H3K27me3. qPCR was used to test the enrichment of the above histone H3 lysine modifications on the promoters of the indicated RP genes.

See also Fig EV5.
Source data are available online for this figure.

© 2021 The Authors

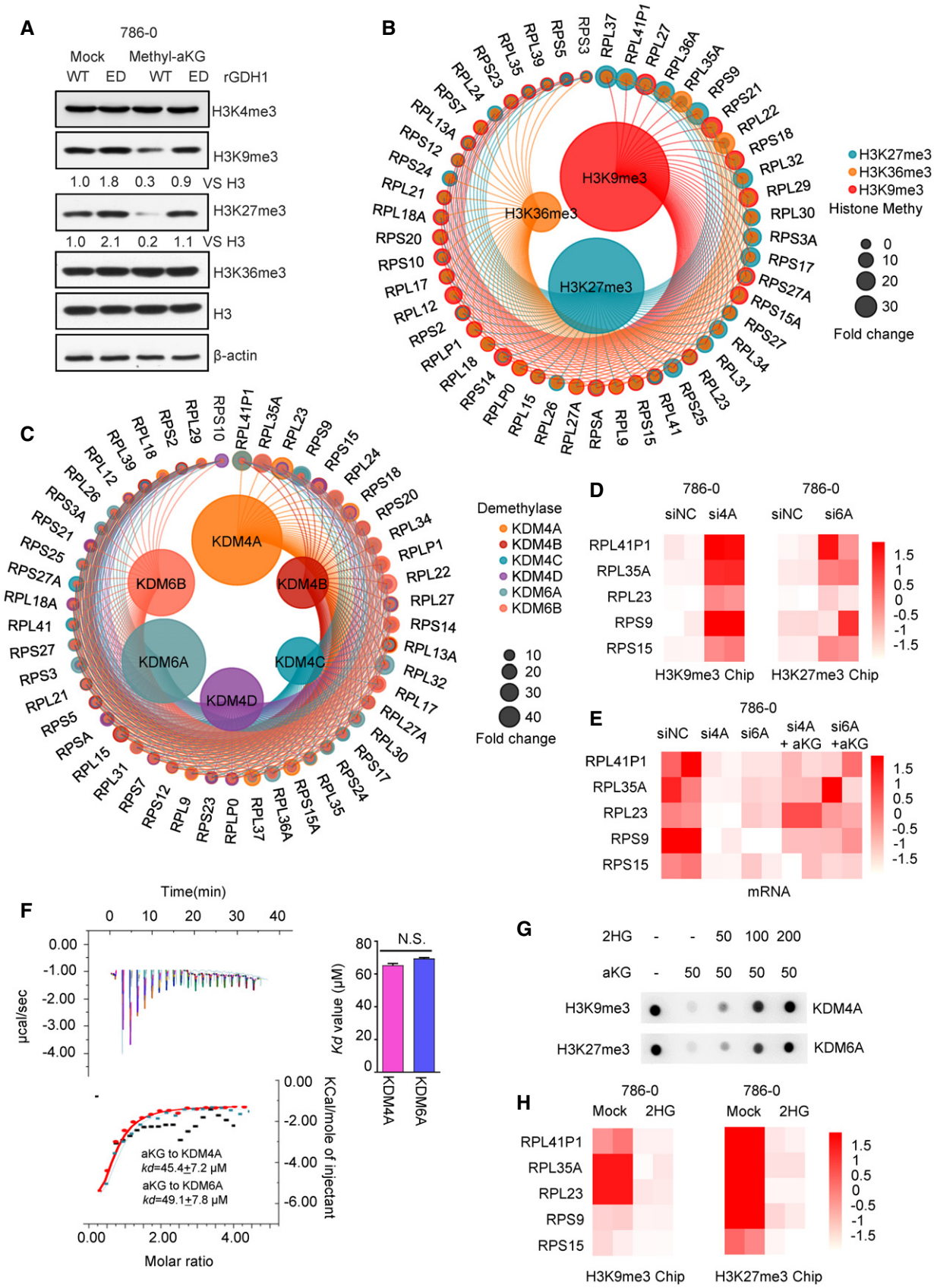

Figure 6.

 © 2021 The Authors

promoting the formation of the inactive state of the promoters of these genes.

Loss of GDH1 or its enzymatic activity or protein stability promotes solid tumor formation

The deprivation of aa reduces cell survival when cells maintain high GDH1 expression. Therefore, we calculated the number of apoptotic cells under aa deprivation using the indicated cells, revealing that a loss of GDH1 or its enzymatic activity promotes cell survival under aa deprivation (Fig 7A). To further uncover the role of GDH1 in solid tumor formation, xenograft tumor growth was tested, calculated, and analyzed. The growth curves and weight of the solid tumors showed that the lack of GDH1 or its enzyme activity promoted the growth of solid tumors, but the enhanced stability of GDH1 inhibited the growth of solid tumors, a finding that was confirmed by Western blotting (Fig 7B–D and Appendix Fig S2A). Both the αKG level and the RP gene expression inversely correlated with the sizes and growth rates of solid tumors, reflecting that higher concentrations of αKG-stimulated RP gene expression were not conducive to the growth of solid tumors (Fig 7E and F). A Ki67 antibody staining assay and TUNEL assay showed cell proliferation and survival in solid tumors, respectively. As expected, the loss of GDH1 or its enzymatic activity helped tumor cells resist apoptosis, while enhanced GDH1 protein stability led to weaker tolerance to stressful environments, such as nutrient-limited environments, during tumor growth (Fig 7G).

Discussion

In addition to autophagy and reinforced uptake of aa, we revealed an economical strategy whereby KIRC cells adapted to quickly respond to aa deprivation and restrained their protein synthesis to retain limited aa, because protein synthesis is considered the most energy-consuming process in the cell. Specifically, when KIRC cells undergo aa deprivation or inhibition of mTORC1, GDH1 translocates from the mitochondria to the cytoplasm and is degraded by the E3 ligase RNF213-mediated ubiquitin degradation pathway. The degradation of GDH1 directs a reduction in intracellular αKG, leading to impaired KDM activity. In the present study, H3K9me3 and H3K27me3 were demethylated by KDM4s and KDM6s, particularly KDM4A and KDM6A, at the promoters of RP genes. Tumor cells actively and coordinately downregulate RP gene expression with an epigenetic way upon aa deprivation. Hence, tumor cells could save the remnant aa for survival. These results shed light on how KIRC cells integrate nutrient availability with coordinated epigenetic gene regulation in response to nutrient limitation (Fig 7H).

Tumor cells perceive the external nutritional environment and reshape their signal transduction to adapt to microenvironmental changes by restricting proliferation (Hanahan & Weinberg, 2011). Whether tumor cells can make these adjustments in a timely manner is an important factor in their progression and survival. We demonstrated that KIRC cells could respond differently according to the abundance of extracellular aa depending on tuning RP gene expression. This finding could be a clever strategy for KIRC cells to adjust their behaviors under an abundant or a limited nutrient supply. However, the present study has drawbacks that must be addressed.

We first observed that the loss of GDH1 conferred tolerance to aa deprivation, which induced the translocation of GDH1 from the mitochondria to the cytoplasm. How do KIRC cells transmit the signal to GDH1 in the mitochondria after sensing the upstream signal of amino acid deficiency? Because aa deprivation restricts the activity of mTORC1, we used inhibitors of the mTORC1 or mTORC1 downstream kinase S6K to treat the cells and obtained similar results as aa deprivation-induced translocation of GDH1. Notably, the deletion of S6K reduced RP gene expression (Chauvin *et al*, 2014); however, a previous study did not show how mTORC1/S6K signals RP gene expression. We preliminarily confirmed that KIRC cells sense aa deprivation through mTORC1, which drives the relocalization of GDH1 in the cytoplasm and that GDH1 degradation supports KIRC cell survival by reducing αKG levels and epigenetic repression of ribosome protein-coding genes and impaired ribosome biogenesis.

As a serine/threonine kinase, the function of mTORC1 depends on its major substrates (Ben-Sahra & Manning, 2017; Liu & Sabatini, 2020). Through its downstream effector S6 kinase and direct target

Figure 7. Loss of GDH1 or its enzymatic activity or its protein stability promotes solid tumor formation, and GDH1 expression is negatively associated with KIRC progression.

A 786-0 cells lacking GDH1 with restored expression of WT, ED, or 3KR mutant GDH1 were subjected to aa starvation for 24 h. PI/Annexin V double staining of the indicated cells was performed, and the number of apoptotic cells in each group was calculated. The data are represented as the mean ± SEM of three independent experiments. Unpaired *t*-test was used with $^{**}P < 0.01$.

B–G Xenogeneic inoculation of 786-0 cells lacking GDH1 with restored expression of WT, ED, or 3KR mutant GDH1 into the left groin of nude mice. The solid tumor formed by the indicated 786-0 cells is shown (B). The tumor growth rate (C), tumor weight (D), and αKG levels in tumors (E) were recorded and analyzed. The tumors were collected to extract total RNA, and qPCR was used to test the mRNA level of the indicated RPL/S genes (F). The staining of Ki67 (G, upper panel) and TUNEL (G, lower panel) using tumors from (B) is shown and analyzed (G, right panel). We used 6 mice in each group. Scale bars: 50 μm.

H Schematic model of the αKG-mediated regulation of RP genes. We uncovered the mechanism by which KIRC cells respond to aa starvation and regulate their protein synthesis to save limited nutrients. Specifically, in KIRC cells under aa starvation, GDH1 is transferred from the mitochondria to the cytoplasm and degraded by the ubiquitin degradation pathway mediated by the E3 ligase RNF213. The degradation of GDH1 directly leads to decreased intracellular αKG, causing the weakened activity of KDM. H3K9me3 and H3K27me3 were demethylated by KDM4 and KDM6, particularly KDM4A and KDM6A, which occupied the promoter of RP genes and cooperatively downregulated the expression of the RP gene during aa starvation. The tumor cells can then preserve the remaining amino acids for survival. Notably, because RP genes are regulated by operons in prokaryotes, we revealed that the expression of most RP genes in renal cell carcinoma cells is mediated by the metabolite αKG.

Data information: (C–E and G) All statistical analyses were conducted using unpaired *t*-test ($n = 6$). (N.S.: not significant; $^{*}P < 0.05$; $^{**}P < 0.01$; $^{***}P < 0.001$). See also Appendix Fig S2.
Source data are available online for this figure.

© 2021 The Authors

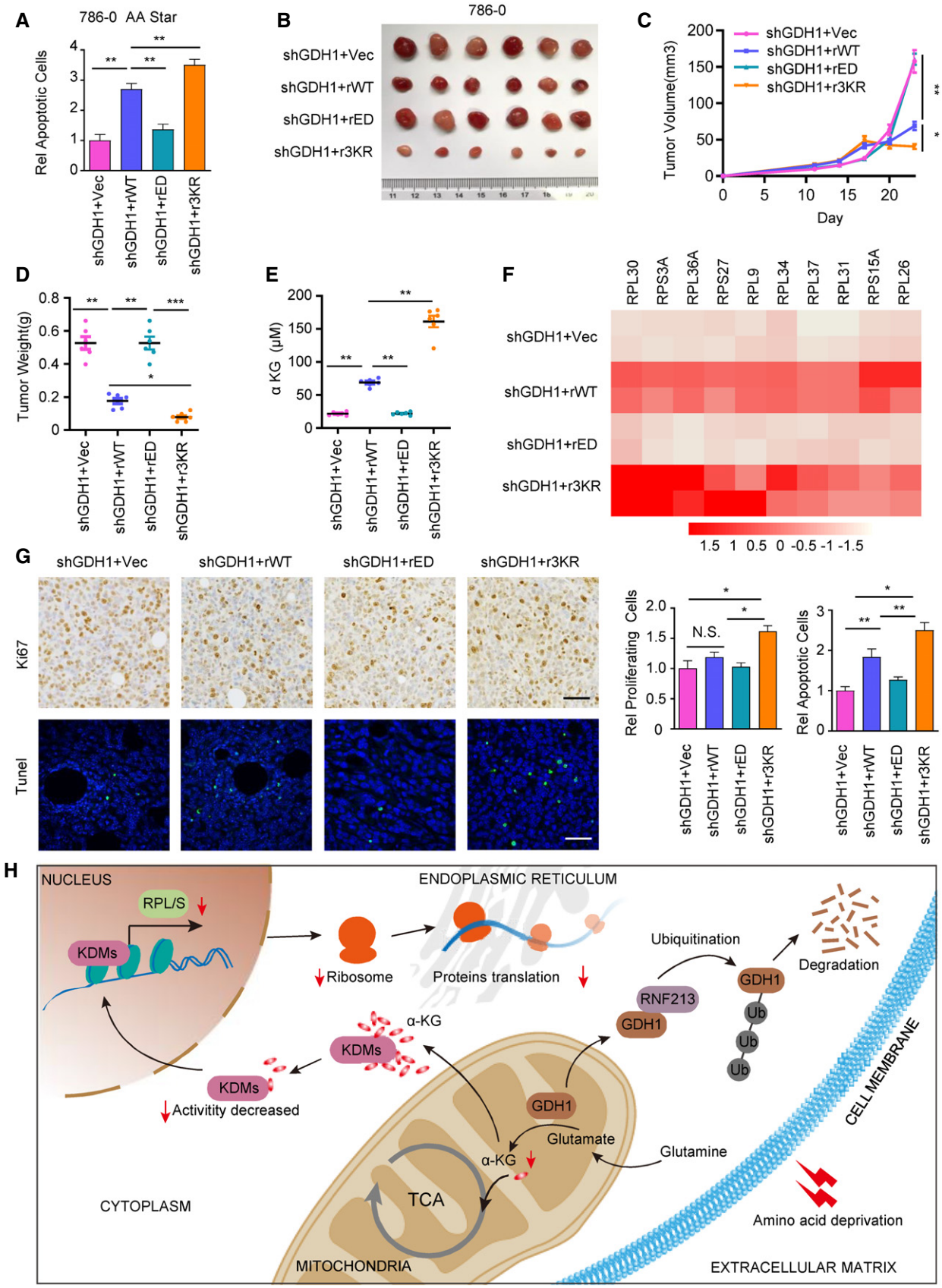

Figure 7.

© 2021 The Authors

4E-binding protein 1 (4E-BP1), mTORC1 regulates protein translation. Through its interaction with the ULK1 (UNC51-like kinase 1)/ATG13 (autophagy 13)/FIP200 (focal adhesion kinase-interacting protein 200 kDa) complex, mTORC1 regulates autophagy (Tan & Miyamoto, 2016; Mossmann *et al*, 2018; Paquette *et al*, 2018). mTORC1 and the mitochondria reciprocally regulate activities and functions. For example, mTORC1 controls mitochondrial activity and biogenesis through 4E-BP-dependent translational regulation (Morita *et al*, 2013), and mTORC1 controls mitochondrial dynamics and cell survival via MTFP1 (mitochondrial fission process 1) (Morita *et al*, 2017). Mitochondrial biogenesis in erythropoiesis is also regulated by mTORC1-mediated protein translation (Liu *et al*, 2017). Considering that mTORC1 is inactivated following amino acid removal, our findings may contribute to understanding the molecular mechanism by which inactivated mTORC1 represses ribosomal biogenesis to reduce the burden and cell survival under nutrition stress through GDH1-mediated RP gene expression. However, the molecular mechanism by which the mTORC1/S6K axis mediates GDH1 translocation remains elusive.

To straight forward discover the effect of GDH1 degradation on RP gene expression, we used an siRNA E3 ligase sublibrary to screen the E3 ligase that ubiquitinates GDH1 and revealed that the RNF213 protein targets GDH1 for proteasomal degradation. To facilitate high-throughput screening, we knocked in GFP onto the C-terminus of GDH1. The real-time screening system records the GFP intensity of GDH1, which would be more reliable than screening interacting E3 ligases by LC-MS/MS. However, this screening method may cause indirect effects. For example, in this study, CHFR and TRIM27 also induced the degradation of the GDH1 protein, but without a direct association between GDH1 and CHFR or TRIM27. The cause may be that CHFR and TRIM27 act on proteins that inhibit the translocation of GDH1, leading to accelerated GDH1 degradation.

RNF213 is a major regulator of moyamoya disease (Kobayashi *et al*, 2015; Ohkubo *et al*, 2015), but few studies have reported on its role in cancers. For example, RNF213 suppresses carcinogenesis in glioblastoma by affecting the MAPK/JNK signaling pathway (Wang *et al*, 2020). RNF213 mutations frequently occur in ARID1A-negative tumors (Kishida *et al*, 2019) and work as novel cancer driver genes and prognostic markers in liver cancer (Li *et al*, 2018). More importantly, RNF213 is a novel PTP1B substrate that regulates oxygen consumption and the survival of $HER2^+$ BC cells in hypoxia (Takeuchi *et al*, 2018). However, whether RNF213 contributes to renal tumorigenesis and protein synthesis remains unclear.

GDH1 is a key enzyme of glutaminolysis that produces αKG through its glutamate dehydrogenation activity. We observed here that amino acid deprivation causes ubiquitination and proteasomal degradation of GDH1 through RNF213, suggesting that GDH1 depletion serves to decrease cellular αKG pools. Consistently, we found that the reduction in RNF213, which mediates GDH1 degradation, restores αKG levels during amino acid deprivation. However, from where might αKG be derived to maintain fundamental cell survival after GDH1 is degraded in aa-starved cells? According to previous reports, macropinocytosis of extracellular proteins can be used to reduce cell dependence on extracellular glutamine. Thus, engulfed proteins, as well as larger macromolecular structures, can then be digested through the action of lysosomal proteases to recover the free amino acid supply for cells under aa deprivation (Commisso *et al*, 2013; Kamphorst *et al*, 2015; Palm *et al*, 2015). Additionally, tumor cells can utilize glucose-derived carbons to maintain TCA cycle anaplerosis and intermediates, thereby contributing to the biosynthesis of glutamate and glutamine (Tardito *et al*, 2015; Davidson *et al*, 2016). Compared with the standard medium, the above two ways may not restore the overall metabolite level under the condition of aa starvation. The maintenance of the αKG level required for cell survival may also be due to the overall weakened metabolic activity of the cells under amino acid deficiency, leading to a reduced requirement of αKG, a finding that is consistent with the reduced cell growth rate in RNF213-depleted cells under aa starvation.

The ribosome, the protein-synthesizing machinery in all cells, comprises approximately 80 RPs and 4 rRNAs in mammals (Klinge & Woolford, 2019). In KIRC cells, we observed that 49 RP genes were coordinately downregulated by GDH1 depletion. However, little is known about how higher eukaryotic ribosomal protein genes are coordinately regulated transcriptionally. Understanding ribosomal protein gene regulation provides novel insight into understanding gene regulatory networks. Although we have clarified that KDM4s and KDM6s, particularly KDM4A and KDM6A, can coordinately affect the downregulated RP genes in the absence of GDH1, we cannot rule out that other KDMs may be involved in regulating RP gene expression.

The expression of RP genes in prokaryotes is controlled by operons (Zengel & Lindahl, 1994). However, the mechanism in higher eukaryotes such as mammals is considerably more complicated. In higher eukaryotes, RP genes are scattered throughout the genome with no operon structure. However, we still observed that RP genes are coordinately expressed in mammalian cells (Hu & Li, 2007). In the present study, the absence of GDH1 leads to the decreased enzyme activity of αKG-dependent KDMs, which occupy the promoter of RP genes and coordinately regulate RP gene expression in KIRC cells. However, the affinity of KDMs binding αKG is different, resulting in distinct degrees of changes in the enzyme activity of KDMs when αKG is downregulated by GDH1 depletion. Our ChIP assay revealed that two or more KDMs occupied the same promoter of RP genes, ensuring that KDMs can demethylate histone lysine methylation on the promoter of RP genes and turn on gene expression.

Different cells rely on distinct metabolic enzymes to maintain αKG homeostasis and present its function. For example, phosphoserine aminotransferase 1 (PSAT1)-produced αKG regulates embryonic stem cell differentiation epigenetically and metabolically (Hwang *et al*, 2016). In glioma cells, the depletion of branched-chain amino acid transaminase 1 (BCAT1) leads to the accumulation of αKG and enhances the activity of αKG-dependent dioxygenases, such as Egl-9 family hypoxia-inducible factor 1 (EGLN1), and further impairs HIF1α protein degradation (Raffel *et al*, 2017). In the present study, GDH1 was the major metabolic enzyme required for αKG production in KIRC cells.

In the TCA cycle, αKG is converted from isocitrate by isocitrate dehydrogenase (IDH). Catalytic arginine mutations in the IDH1 and IDH2 genes found in gliomas and acute myeloid leukemia (AML) result in neomorphic enzymes that, instead, convert αKG to the structurally similar R-2HG, which accumulates to exceedingly high levels in these patients (Dang *et al*, 2009; Gross *et al*, 2010; Ward *et al*, 2010). R-2HG is now considered an oncometabolite, impairing

© 2021 The Authors

epigenetic and hypoxic regulation by binding to αKG-dependent dioxygenases (Figueroa *et al*, 2010; Xu *et al*, 2011), while previous reports show potential antitumor activity (Fu *et al*, 2015; Su *et al*, 2018). In the present study, R-2HG facilitated KIRC cell survival following aa deprivation. Specifically, R-2HG competes for the binding of αKG to KDMs, thereby inhibiting the enzymatic activity of KDMs and further reducing the expression of RP genes. Hence, we suspect that the oncometabolic or suppressive role of R-2HG partially depends on the role of αKG in cancers.

In conclusion, following aa deprivation, KIRC cells adopt an economical and efficient strategy to quickly switch from proliferation to survival depending on the GDH1/RNF213/KDMs/RP axis and avoid autophagy, which consumes ATP and NADH/NADPH. Additionally, our data show that this strategy mainly relies on αKG-dependent KDMs, which epigenetically and coordinately regulate RP gene expression accompanied by adjusting protein synthesis according to the abundance of extracellular aa. Therefore, inhibiting the signal transduction of the above axis by delivering cell-permeable αKG would be an efficient method for the targeted inhibition of KIRC progression.

Materials and Methods

Clinical specimens

Primary KIRC specimens from patients with or without recurrence were collected from Shanghai First People's Hospital, Shanghai Jiao Tong University, Shanghai, China. The use of clinical samples was approved by the institutional review board of the hospital. All the clinical samples were collected with informed consent under Health Insurance Portability and Accountability Act (HIPAA)-approved protocols.

Cell lines, antibodies, and reagents

The cell lines were obtained from the SIBCB (Institute of Biochemistry and Cell Biology, SIBS, CAS, China) cell collection or American Type Culture Collection (ATCC catalog numbers: 786-0, 769-P and HEK293T cells). The cells were authenticated using the short tandem repeat (STR) method.

Reagents

Lipofectamine 3000 was obtained from Invitrogen (Carlsbad, CA, USA). Trypan blue solution (T8154), dimethyl 2-oxoglutarate (349631), octyl-(R)-2HG (SML2200), CQ (C6628), and MG132 (M7449) were purchased from Sigma-Aldrich. RIPA lysis buffer, puromycin, and hygromycin were purchased from Merck/Millipore (Darmstadt, Germany). Torin 1 (#14379) was purchased from Cell Signaling Technology. MitoTracker Red (M7512) was purchased from Thermo Fisher Scientific (China, Shanghai). All the methylation states (me2 and me3) of H3K9, H3K27, and H3K36 were synthesized by GenScript (China, Nanjing), and high-performance liquid chromatography (HPLC) was performed to achieve greater than 95% purity.

The primary antibodies used were as follows: Mouse monoclonal antibodies against HA, Flag, anti-Flag M2 affinity gel, β-actin, and tubulin were purchased from Sigma (St. Louis, MO, USA). Rabbit polyclonal antibodies against GDH1 (14299-1-AP), VDAC1 (PA1-954A), RNF213 (A305-841A-M), CHFR (PA5-106807), TRIM27 (PA5-65785), RPL30 (PA5-89360), RPL36A (PA5-64144), RPS3A (PA5-29398), RPS27 (PA5-79936), RPL9 (PA5-51915), RPL34 (PA5-57173), RPL37 (PA5-78154), RPL31 (PA5-104549), RPS15A (PA5-51314), and RPL26 (PA5-95828) were purchased from Thermo Fisher Scientific (Shanghai, China).

The secondary antibodies goat anti-mouse IgG HRP (G-21040) and goat anti-rabbit HRP (G-21234) were purchased from Thermo Fisher Scientific (Shanghai, China). Goat anti-rabbit Alexa Fluor® 568 (ab175473) and goat anti-mouse Alexa Fluor® 555 (ab150118) were purchased from Abcam.

Commercial recombinant KDM4A (31457) and KDM6A/UTX (31460) were purchased from Active Motif (Shanghai, China).

Chromatin immunoprecipitation (IP) antibodies against H3K9me3 (07-442), H3K27me3 (07-449), H3K36me3 (ABE435) and H3K4me3 (07-473), KDM4A (MABN685), KDM4A/JMJD2A (ABS462), and KDM6A/UTX (MABE201) were purchased from Millipore (Darmstadt, Germany). KDM4C/JMJD2C (ab27532), KDM4D/JMJD2D (ab93694), and KDM6B/JMJD3 (ab38113) were purchased from Abcam (Cambridge, MA, UK). IP and immunoblotting (IB) analyses were performed as described (Wang *et al*, 2017). Notably, antibodies for IB were diluted 1:1,000; for IP or chromatin IP, we used 5 μg for each sample; and for IF or IHC, the antibodies were diluted 1:100 or 1:200. Extraction of total proteins using a modified RIPA lysis buffer was followed by IP and IB using the indicated antibodies. Protein levels were quantified using densitometry.

siRNAs targeting RNF213 (140684), KDM4A (148456), and KDM6A/UTX (139855) were purchased from Thermo Fisher Scientific (Shanghai, China).

Plasmids, lentivirus packaging, and infection

The plasmids expressing GDH1 in mammalian cells and *E. coli* and knocking down GDH1 were described in a previous report (Wang *et al*, 2019). The mitochondrial signal peptide of GDH1 was deleted from amino acids 1–15. GDH1 mutagenesis was generated using the QuickChange site-directed mutagenesis kit (Stratagene, La Jolla, CA, USA). For shRNA-resistant clones, PCR products containing 4 synonymous mutations in the middle of the shRNA-targeted sequence were generated and subcloned into non-tagged pCDH-hygromycin vectors.

Lentivirus amplification was performed using standard methods in subconfluent HEK293T cells. Infection of renal cancer cell lines was performed in the presence of polybrene (Sigma) at a final concentration of 8 $\mu g\,ml^{-1}$. Cells were incubated with a lentivirus mixture for 72 h, digested with trypsin in fresh growth medium, and then were sorted using green fluorescence for stable expression or knockdown. The constructed stable cell lines were amplified and saved for future experiments.

Amino acid (aa) starvation

To achieve aa starvation in tumor cells, we removed some amino acids from the culture medium according to a previous report (Demetriades *et al*, 2014). Medium for the aa starvation experiment was prepared using Earle's balanced salt solution (EBSS) supplemented with 1 mM sodium pyruvate and 4× MEM vitamin solution.

 © 2021 The Authors

The control medium was also supplemented with 0.4 mM glycine, 0.4 mM L-arginine, 0.2 mM L-cystine, 4.0 mM L-glutamine, 0.2 mM L-histidine, 0.8 mM L-isoleucine, 0.8 mM L-leucine, 0.8 mM L-lysine, 0.2 mM L-methionine, 0.4 mM L-phenylalanine, 0.4 mM L-serine, 0.8 mM L-threonine, 0.08 mM L-tryptophan, 0.4 mM L-tyrosine, and 0.8 mM L-valine (Sigma-Aldrich, USA). Both media were supplemented with 5% FBS that had been dialyzed using a 3500 Da cutoff membrane (Spectrumlabs; 132720).

Notably, to quickly achieve the effect of aa starvation after removing the DMEM medium, the cells were washed twice with PBS before adding aa starvation medium.

Transfection

The cells were seeded into 60-mm or 100-mm plates and then were transfected with the indicated plasmids using PolyJet according to the manufacturer's instructions.

Cell viability assay

In total, 2×10^5 786-0 or 769-P cells with or without genetic modifications were plated in DMEM or aa starvation medium for the indicated time. Cell viability was determined by Trypan blue staining.

RNA sequencing and analysis

Total RNA was extracted for RNA sequencing using an Illumina HiSeq 2500 sequencing instrument. Sequencing data analysis and management were performed using the BaseSpace Sequence Hub. KEGG pathway analysis was performed using clusterProfiler software (Yu *et al*, 2012), and the plot was generated using ggplot2 in R (3.5.0). GSEA was performed using GSEA software (v4.1.0) as previously described (Subramanian *et al*, 2005).

qRT–PCR

Quantitative real-time (qRT) PCR analysis was performed using 2× SYBR real-time PCR Premixture (Roche) under the following conditions: 5 min at 95°C followed by 40 cycles at 95°C for 30 s, 55°C for 40 s, and 72°C for 1 min using an ABI Prism 7700 sequence detection system. The data were normalized to the expression of a control gene (ACTN) for each experiment. The data are represented as means ± SD of three independent experiments. The primer pairs used for quantitative real-time PCR are listed in Appendix Table S1.

Protein synthesis assay

Protein synthesis was evaluated using the Cayman kit (601100). Briefly, tumor cells were pretreated with or without aa starvation for the indicated time and incubated with cycloheximide for 30 min at 37°C. The cells were collected and incubated with OPP working solution for 30 min at 37°C. Next, the cells were treated with fixative buffer (Item No. 10009899) and wash buffer (Item No. 10009866). The cells were spun down, resuspended in FAM-Azide staining solution, and incubated in the dark for 30 min. Finally, the cells were spun down, resuspended in assay buffer, and immediately analyzed with a flow cytometer capable of detecting FITC at excitation/emission = 483 nm/525 nm. Coomassie Brilliant Blue (CBB) staining, BCA assay, and Western blotting were performed to confirm the total proteins or target protein level, respectively.

Western blotting (WB)

After different treatments, the tumor cells were lysed, and the protein concentration was determined using the Bradford assay. Total or immunoprecipitated proteins were separated by SDS–PAGE and detected using the indicated antibodies.

TCGA kidney renal clear cell carcinoma cohort data analysis

TCGA kidney renal clear cell carcinoma (KIRC) datasets were collected from the UCSC Xena multiomics database platform (https://tcga.xenahubs.net; preprint: Goldman *et al*, 2019), which included the patients' clinically annotated phenotypes (n = 944) and corresponding RNA sequencing transcriptomic features (n = 606). The KIRC mRNA expression profile within the UCSC Xena platform was preprocessed, annotated, and normalized (preprint: Goldman *et al*, 2019). Therefore, based on the matched TCGA sample IDs of these data, we could stratify these KIRC samples into two groups (primary tumors versus adjacent normal tissues, based on the "sample type" phenotype) and four stages (Stages I, II, III, and IV, based on AJCC staging criteria). We also divided the samples into non-metastasis (M0) and metastasis (M1) groups using the criteria established by the American Joint Committee on Cancer (AJCC). Next, the GDH1 mRNA expression values between different groups (t-test) or stages (ANOVA) were compared, and the significance was determined using the p-value. Based on the GDH1 mRNA expression values, the samples were divided into GDH1 high (n = 262) and low (n = 268) groups by the median value. The overall survival curve between the GDH1 high and low groups was plotted according to the matched clinical data. The plots were generated using R (3.5.0).

Immunohistochemistry (IHC)

The tissue sections from paraffin-embedded human KIRC specimens were stained with antibodies as indicated, and we quantitatively scored the tissue sections according to the percentage of positive cells and staining intensity, as described previously (Wang *et al*, 2019). The scores were compared with overall survival, defined as the time from the date of diagnosis to death or the last known date of follow-up.

Subcellular fractionation

To obtain subcellular fractions, 786-0 or 769-P cells were harvested and washed three times with cold PBS. Cytosolic or mitochondrial fractions were prepared using the Mitochondria/Cytosol Fraction Kit (BioVision).

Immunoprecipitation (IP) and LC-MS/MS analysis of ubiquitin

Immunoprecipitation (IP) for flag-tagged GDH1 from 786-0 or 769-P cells and separation by SDS–PAGE were previously described (Wang *et al*, 2019). Samples from SDS–PAGE were digested by trypsin, and peptides were analyzed using a nanoflow HPLC Easy-nLC 1000

© 2021 The Authors

system coupled to a Q Exactive HF mass spectrometer (Thermo Fisher Scientific). The MS raw data were analyzed using Proteome Discoverer 2.3 against the human Swiss-Prot database containing 20,231 sequences (downloaded in December 2017). Carbamidomethyl cysteine was searched as a fixed modification. Oxidized methionine, protein N-terminal acetylation, and lysine ubiquitination residue (GlyGly) were set as variable modifications. The spectra containing lysine GlyGly modifications were extracted from the database search results.

GDH1 enzymatic assay

GDH1 activity as a dehydrogenase was measured as described previously (Wang *et al*, 2019). Briefly, GDH1 was immunoprecipitated from the lysates of KIRC cells and subjected to GDH1 enzymatic activity assays in reaction buffer containing 100 mM Tris (pH 8.0), 50 mM L-glutamic acid, and 1 mM NAD^+. The change in absorbance at 340 nm due to increased NADH was measured using a BioTek Synergy Neo Multi-Mode Plate Reader (BioTek, USA).

siRNA screen E3 ligase for GDH1 degradation

To screen E3 ligases for GDH1 degradation, 786-0 cells were plated in 96-well plates. When the cell confluency reached 50%, the cells were transfected with individual siRNAs that targeted 335 E3 ligases (three siRNAs per gene; indicated as "siGene" on the x-axis) into cells for 48 h and treated with aa starvation for 12 h. The fluorescence of GDH1-GFP in each well was recorded using Opera Phenix (Perkin Elmer) at the time points of the starting point and aa starvation for 12 h. The data analyses are described in the legend.

In vitro ubiquitin assay

His-GDH1 (including WT and 3KR mutant) was purified from BL21 (DE3) cells. FLAG-RNF213 was pulled down from HEK293T cells and washed twice with cold PBS with 1% NP40, removing the associated proteins of RNF213. Ubiquitin-activating enzyme E1 and ubiquitin-conjugating enzyme E2 were commercially purchased. The reaction (Zhao *et al*, 2012) was mixed by vortexing briefly and incubating with FLAG-RNF213 and His-GDH1. The reaction was terminated by adding sample buffer and boiling for 4 min at 95°C with SDS-loading buffer. WB was used to measure the level of GDH1 ubiquitin using the indicated antibodies.

αKG and R-2HG determination

The adherent cells were digested by trypsin for 1–2 min, and the xenograft tumors from Fig 7B were digested by collagenase IV for 30–60 min. Fifty microliters of tumor cells were collected in an Eppendorf tube (500 μl) with a scale (the scale was also accomplished by pipettes in which 50 μl of water was drawn into an Eppendorf tube, and we marked the volume as 50 μl in the tube wall). Next, the concentration of αKG was measured using an αKG assay kit (colorimetric) (Sigma-Aldrich, MAK054) according to the manufacturer's instructions. R-2HG levels were determined using the D-2-Hydroxyglutarate Assay Kit (Colorimetric) (K213-100, BioVision).

Chromatin immunoprecipitation

Chromatin immunoprecipitation (ChIP) assays were performed as previously described (Carey *et al*, 2009). Rabbit or mouse monoclonal antibodies against H3K9me3, H3K27me3, H3K36me3, KDM4A-4D, or KDM6A-6B were used in the ChIP assays, with rabbit monoclonal IgG serving as a negative control. The enrichment of H3K9me3, H3K27me3, H3K36me3, KDM4A-4D, or KDM6A-6B on RP gene promoters was assessed by quantitative RT-PCR. The input was 1% sonicated DNA before the addition of antibodies. The sequences of the primers for RP gene promoters are provided in Appendix Table S1.

KDM enzymatic assay

Commercial KDMs were incubated using the corresponding substrate (peptides containing lysine methylation modification) in reaction buffer (40 mM Tris–HCl, pH 8, 100 mM NaCl, 2 mM KCl, 1 mM dithiothreitol, 1 mM EDTA, and 0.05% Tween-20) at room temperature for 30 min. The dot blot assay was performed using the indicated antibodies against H3K9me2/3, H3K27me2/3, or H3K36me2/3.

Isothermal titration calorimetry (ITC)

The thermodynamic parameters of the binding of αKG or R-2HG to KDMs were measured by ITC assays using the ITC200 Microcalorimeter (MicroCal) at 25°C, and the detailed process was previously described (Wang *et al*, 2019). Briefly, in all the experiments, the initial injection of 0.5 ml of αKG or R-2HG solution was discarded to eliminate the effect of titrant diffusion across the syringe tip during the equilibration process, and each dataset comprised 20 injections of 2 ml each of 1 mM αKG into the sample cell containing 250 ml of 0.05 mM KDMs. The heat of dilution was negligible in all cases. The binding constant and other thermodynamic parameters were determined by fitting the integrated titration data using the single binding site model in the nonlinear least-squares method and MicroCal Origin software (version 7.0).

Apoptosis assay

Flow cytometry analyses for cell death were detected using an Annexin V-fluorescein isothiocyanate (FITC)/PI kit as described previously (Shao *et al*, 2019). After treatment, the cells were trypsinized, collected by centrifugation, washed with PBS, and resuspended in Annexin V binding buffer. Next, Annexin V-FITC conjugates and PI solution were incubated together for 15 min in the dark. Finally, the cells were incubated with Annexin V binding buffer and analyzed within 1 h by flow cytometric analysis (BD FACS Aria SORP). Notably, 20,000 cells were analyzed to determine the percentage of apoptotic cells.

Xenograft study

Briefly, 2×10^6 786-0-derived stable cells (Fig 7) were subcutaneously injected into the left dorsal area of randomized 6-week-old female athymic nude mice. After inoculation for 24 days, the mice were euthanized, and the tumors were dissected. Differences in the

 © 2021 The Authors

weight, growth rate, and αKG level of xenograft tumors were statistically analyzed.

Statistical analysis

Statistical analysis was performed using the Statistical Package for the Social Sciences (SPSS) software version 12 for Windows (SPSS Inc., Chicago, IL, USA). Student's *t*-test was used to determine the statistical significance of the differences between the experimental groups. A $P < 0.05$ was considered significant. Graphs were created using Microcal Origin software (version 3.78; Microcal Software Inc., Northampton, MA, USA). We used the TCGA-KIRC cohort to assess the association of GDH1 or RNF213 expression with overall survival (split patients by best; follow-up threshold: 180 months).

Data availability

RNA-Seq data: Gene Expression Omnibus GSE167514 (https://www.ncbi.nlm.nih.gov/geo/query/acc.cgi?acc=GSE167514).

Expanded View for this article is available online.

Acknowledgements
The authors thank the CAS Shanghai Institute of Nutrition and Health (SINH) Molecular and metabolism core facility for the metabolite determination and protein synthesis service. This study was supported in part by NSFC grant Nos. 92053113 and 81570607, National Natural Science Foundation for Young Scholars of China (Nos. 81902566 and 81902863), and Shanghai Jiao Tong University Medical-Engineering Cross Research Fund (No. YG2019QNA53).

Author contributions
JS, TS, YD, and HY designed, performed, and analyzed the experiments and prepared the figures. LL provided technical help. XJW conceived this study and wrote the manuscript, and HY rewrote the revised manuscript. XW and XJW designed and analyzed the experiments and wrote the manuscript.

Conflicts of interest
The authors declare that they have no conflict of interest.

References

Baksh SC, Todorova PK, Gur-Cohen S, Hurwitz B, Ge Y, Novak JSS, Tierney MT, Dela Cruz-Racelis J, Fuchs E, Finley LWS (2020) Extracellular serine controls epidermal stem cell fate and tumour initiation. *Nat Cell Biol* 22: 779 – 790

Ben-Sahra I, Manning BD (2017) mTORC1 signaling and the metabolic control of cell growth. *Curr Opin Cell Biol* 45: 72 – 82

Bento CF, Renna M, Ghislat G, Puri C, Ashkenazi A, Vicinanza M, Menzies FM, Rubinsztein DC (2016) Mammalian autophagy: how does it work? *Annu Rev Biochem* 85: 685 – 713

Berry WL, Janknecht R (2013) KDM4/JMJD2 histone demethylases: epigenetic regulators in cancer cells. *Can Res* 73: 2936 – 2942

Carey MF, Peterson CL, Smale ST (2009) Chromatin Immunoprecipitation (ChIP). *Cold Spring Harbor Protocols* 2009(9): pdb.prot5279

Carrer A, Wellen KE (2015) Metabolism and epigenetics: a link cancer cells exploit. *Curr Opin Biotechnol* 34: 23 – 29

Catez F, Dalla Venezia N, Marcel V, Zorbas C, Lafontaine DLJ, Diaz JJ (2019) Ribosome biogenesis: an emerging druggable pathway for cancer therapeutics. *Biochem Pharmacol* 159: 74 – 81

Chaillou T, Kirby TJ, McCarthy JJ (2014) Ribosome biogenesis: emerging evidence for a central role in the regulation of skeletal muscle mass. *J Cell Physiol* 229: 1584 – 1594

Chauvin C, Koka V, Nouschi A, Mieulet V, Hoareau-Aveilla C, Dreazen A, Cagnard N, Carpentier W, Kiss T, Meyuhas O *et al* (2014) Ribosomal protein S6 kinase activity controls the ribosome biogenesis transcriptional program. *Oncogene* 33: 474 – 483

Clausen L, Abildgaard AB, Gersing SK, Stein A, Lindorff-Larsen K, Hartmann-Petersen R (2019) Protein stability and degradation in health and disease. *Adv Protein Chem Struct Biol* 114: 61 – 83

Commisso C, Davidson SM, Soydaner-Azeloglu RG, Parker SJ, Kamphorst JJ, Hackett S, Grabocka E, Nofal M, Drebin JA, Thompson CB *et al* (2013) Macropinocytosis of protein is an amino acid supply route in Ras-transformed cells. *Nature* 497: 633 – 637

Dang L, White DW, Gross S, Bennett BD, Bittinger MA, Driggers EM, Fantin VR, Jang HG, Jin S, Keenan MC *et al* (2009) Cancer-associated IDH1 mutations produce 2-hydroxyglutarate. *Nature* 462: 739 – 744

Davidson S, Papagiannakopoulos T, Olenchock B, Heyman J, Keibler M, Luengo A, Bauer M, Jha A, O'Brien J, Pierce K *et al* (2016) Environment impacts the metabolic dependencies of Ras-driven non-small cell lung cancer. *Cell Metab* 23: 517 – 528

DeLuna A, Avendano A, Riego L, Gonzalez A (2001) NADP-glutamate dehydrogenase isoenzymes of Saccharomyces cerevisiae. Purification, kinetic properties, and physiological roles. *J Biol Chem* 276: 43775 – 43783

Demetriades C, Doumpas N, Teleman AA (2014) Regulation of TORC1 in response to amino acid starvation via lysosomal recruitment of TSC2. *Cell* 156: 786 – 799

Dimitrova E, Turberfield AH, Klose RJ (2015) Histone demethylases in chromatin biology and beyond. *EMBO Rep* 16: 1620 – 1639

DiNardo CD, Propert KJ, Loren AW, Paietta E, Sun Z, Levine RL, Straley KS, Yen K, Patel JP, Agresta S *et al* (2013) Serum 2-hydroxyglutarate levels predict isocitrate dehydrogenase mutations and clinical outcome in acute myeloid leukemia. *Blood* 121: 4917 – 4924

Figueroa ME, Abdel-Wahab O, Lu C, Ward PS, Patel J, Shih A, Li Y, Bhagwat N, Vasanthakumar A, Fernandez HF *et al* (2010) Leukemic IDH1 and IDH2 mutations result in a hypermethylation phenotype, disrupt TET2 function, and impair hematopoietic differentiation. *Cancer Cell* 18: 553 – 567

Fu X, Chin R, Vergnes L, Hwang H, Deng G, Xing Y, Pai M, Li S, Ta L, Fazlollahi F *et al* (2015) 2-Hydroxyglutarate inhibits ATP synthase and mTOR signaling. *Cell Metab* 22: 508 – 515

Goldman M, Craft B, Hastie M, Repečka K, Kamath A, McDade F, Rogers D, Brooks AN, Zhu J, Haussler D (2019) The UCSC Xena platform for public and private cancer genomics data visualization and interpretation. *bioRxiv* https://doi.org/10.1101/326470 [PREPRINT]

Goold R, McKinnon C, Tabrizi SJ (2015) Prion degradation pathways: Potential for therapeutic intervention. *Mol Cell Neurosci* 66: 12 – 20

Gross S, Cairns RA, Minden MD, Driggers EM, Bittinger MA, Jang HG, Sasaki M, Jin S, Schenkein DP, Su SM *et al* (2010) Cancer-associated metabolite 2-hydroxyglutarate accumulates in acute myelogenous leukemia with isocitrate dehydrogenase 1 and 2 mutations. *J Exp Med* 207: 339 – 344

Hanahan D, Weinberg RA (2011) Hallmarks of cancer: the next generation. *Cell* 144: 646 – 674

Hancock RL, Dunne K, Walport LJ, Flashman E, Kawamura A (2015) Epigenetic regulation by histone demethylases in hypoxia. *Epigenomics* 7: 791 – 811

© 2021 The Authors

Hu H, Li X (2007) Transcriptional regulation in eukaryotic ribosomal protein genes. *Genomics* 90: 421 – 423

Hwang IY, Kwak S, Lee S, Kim H, Lee SE, Kim JH, Kim YA, Jeon YK, Chung DH, Jin X *et al* (2016) Psat1-dependent fluctuations in alpha-ketoglutarate affect the timing of ESC differentiation. *Cell Metab* 24: 494 – 501

Iadevaia V, Liu R, Proud CG (2014) mTORC1 signaling controls multiple steps in ribosome biogenesis. *Semin Cell Dev Biol* 36: 113 – 120

Islam MS, Leissing TM, Chowdhury R, Hopkinson RJ, Schofield CJ (2018) 2-oxoglutarate-dependent oxygenases. *Annu Rev Biochem* 87: 585 – 620

Kamphorst JJ, Nofal M, Commisso C, Hackett SR, Lu W, Grabocka E, Vander Heiden MG, Miller G, Drebin JA, Bar-Sagi D *et al* (2015) Human pancreatic cancer tumors are nutrient poor and tumor cells actively scavenge extracellular protein. *Cancer Res* 75: 544 – 553

Kishida Y, Oishi T, Sugino T, Shiomi A, Urakami K, Kusuhara M, Yamaguchi K, Kitagawa Y, Ono H (2019) Associations between loss of ARID1A expression and clinicopathologic and genetic variables in T1 early colorectal cancer. *Am J Clin Pathol* 152: 463 – 470

Klinge S, Woolford Jr JL (2019) Ribosome assembly coming into focus. *Nat Rev Mol Cell Biol* 20: 116 – 131

Kobayashi H, Matsuda Y, Hitomi T, Okuda H, Shioi H, Matsuda T, Imai H, Sone M, Taura D, Harada KH *et al* (2015) Biochemical and functional characterization of RNF213 (Mysterin) R4810K, a susceptibility mutation of moyamoya disease, in angiogenesis *in vitro* and *in vivo*. *J Am Heart Assoc* 4: e002146

Kotzamani D, Plaitakis A (2012) Alpha helical structures in the leader sequence of human GLUD2 glutamate dehydrogenase responsible for mitochondrial import. *Neurochem Int* 61: 463 – 469

Lamadema N, Burr S, Brewer AC (2019) Dynamic regulation of epigenetic demethylation by oxygen availability and cellular redox. *Free Radic Biol Med* 131: 282 – 298

Legendre F, MacLean A, Appanna VP, Appanna VD (2020) Biochemical pathways to alpha-ketoglutarate, a multi-faceted metabolite. *World J Microbiol Biotechnol* 36: 123

Li X, Xu W, Kang W, Wong SH, Wang M, Zhou Y, Fang X, Zhang X, Yang H, Wong CH *et al* (2018) Genomic analysis of liver cancer unveils novel driver genes and distinct prognostic features. *Theranostics* 8: 1740 – 1751

Liu GY, Sabatini DM (2020) mTOR at the nexus of nutrition, growth, ageing and disease. *Nat Rev Mol Cell Biol* 21: 183 – 203

Liu X, Zhang Y, Ni M, Cao H, Signer RAJ, Li D, Li M, Gu Z, Hu Z, Dickerson KE *et al* (2017) Regulation of mitochondrial biogenesis in erythropoiesis by mTORC1-mediated protein translation. *Nat Cell Biol* 19: 626 – 638

Lorenzo FR, Huff C, Myllymäki M, Olenchock B, Swierczek S, Tashi T, Gordeuk V, Wuren T, Ri-Li Ge, McClain DA *et al* (2014) A genetic mechanism for Tibetan high-altitude adaptation. *Nat Genet* 46: 951 – 956

Ma XM, Blenis J (2009) Molecular mechanisms of mTOR-mediated translational control. *Nat Rev Mol Cell Biol* 10: 307 – 318

McBrayer SK, Mayers JR, DiNatale GJ, Shi DD, Khanal J, Chakraborty AA, Sarosiek KA, Briggs KJ, Robbins AK, Sewastianik T *et al* (2018) Transaminase inhibition by 2-hydroxyglutarate impairs glutamate biosynthesis and redox homeostasis in glioma. *Cell* 175: 101 – 116

Morita M, Gravel S-P, Chénard V, Sikström K, Zheng L, Alain T, Gandin V, Avizonis D, Arguello M, Zakaria C *et al* (2013) mTORC1 controls mitochondrial activity and biogenesis through 4E-BP-dependent translational regulation. *Cell Metab* 18: 698 – 711

Morita M, Prudent J, Basu K, Goyon V, Katsumura S, Hulea L, Pearl D, Siddiqui N, Strack S, McGuirk S *et al* (2017) mTOR controls mitochondrial dynamics and cell survival via MTFP1. *Mol Cell* 67: 922 – 935

Mosammaparast N, Shi Y (2010) Reversal of histone methylation: biochemical and molecular mechanisms of histone demethylases. *Annu Rev Biochem* 79: 155 – 179

Mossmann D, Park S, Hall MN (2018) mTOR signalling and cellular metabolism are mutual determinants in cancer. *Nat Rev Cancer* 18: 744 – 757

Mullen A, Hu Z, Shi X, Jiang L, Boroughs L, Kovacs Z, Boriack R, Rakheja D, Sullivan L, Linehan W *et al* (2014) Oxidation of alpha-ketoglutarate is required for reductive carboxylation in cancer cells with mitochondrial defects. *Cell Rep* 7: 1679 – 1690

Ohkubo K, Sakai Y, Inoue H, Akamine S, Ishizaki Y, Matsushita Y, Sanefuji M, Torisu H, Ihara K, Sardiello M *et al* (2015) Moyamoya disease susceptibility gene RNF213 links inflammatory and angiogenic signals in endothelial cells. *Sci Rep* 5: 13191

Palm W, Park Y, Wright K, Pavlova NN, Tuveson DA, Thompson CB (2015) The utilization of extracellular proteins as nutrients is suppressed by mTORC1. *Cell* 162: 259 – 270

Paquette M, El-Houjeiri L, Pause A (2018) mTOR pathways in cancer and autophagy. *Cancers* 10: 18

Plaitakis A, Metaxari M, Shashidharan P (2000) Nerve tissue-specific (GLUD2) and housekeeping (GLUD1) human glutamate dehydrogenases are regulated by distinct allosteric mechanisms: implications for biologic function. *J Neurochem* 75: 1862 – 1869

Rabanal-Ruiz Y, Otten EG, Korolchuk VI (2017) mTORC1 as the main gateway to autophagy. *Essays Biochem* 61: 565 – 584

Rabinowitz JD, White E (2010) Autophagy and metabolism. *Science* 330: 1344 – 1348

Raffel S, Falcone M, Kneisel N, Hansson J, Wang W, Lutz C, Bullinger L, Poschet G, Nonnenmacher Y, Barnert A *et al* (2017) BCAT1 restricts alphaKG levels in AML stem cells leading to IDHmut-like DNA hypermethylation. *Nature* 551: 384 – 388

Reiter-Brennan C, Semmler L, Klein A (2018) The effects of 2-hydroxyglutarate on the tumorigenesis of gliomas. *Contemp Oncol* 22: 215 – 222

Rose NR, McDonough MA, King ON, Kawamura A, Schofield CJ (2011) Inhibition of 2-oxoglutarate dependent oxygenases. *Chem Soc Rev* 40: 4364 – 4397

Rosenblum G, Chen C, Kaur J, Cui X, Goldman YE, Cooperman BS (2012) Real-time assay for testing components of protein synthesis. *Nucleic Acids Res* 40: e88

Saxton RA, Sabatini DM (2017) mTOR signaling in growth, metabolism, and disease. *Cell* 169: 361 – 371

Shao J, Lu J, Zhu W, Yu H, Jing X, Wang YL, Wang X, Wang XJ (2019) Derepression of LOXL4 inhibits liver cancer growth by reactivating compromised p53. *Cell Death Differ* 26: 2237 – 2252

Shpargel KB, Starmer J, Yee D, Pohlers M, Magnuson T (2014) KDM6 demethylase independent loss of histone H3 lysine 27 trimethylation during early embryonic development. *PLoS Genet* 10: e1004507

Su R, Dong L, Li C, Nachtergaele S, Wunderlich M, Qing Y, Deng X, Wang Y, Weng X, Hu C *et al* (2018) R-2HG exhibits anti-tumor activity by targeting FTO/m(6)A/MYC/CEBPA signaling. *Cell* 172: 90 – 105

Subramanian A, Tamayo P, Mootha Vk, Mukherjee S, Ebert Bl, Gillette Ma, Paulovich A, Pomeroy Sl, Golub Tr, Lander Es *et al* (2005) Gene set enrichment analysis: a knowledge-based approach for interpreting genome-wide expression profiles. *Proc Natl Acad Sci USA* 102: 15545 – 15550

Takeuchi J, Kataoka K, Ito Y, Takayama K, Yasuma T, Kaneko H, Terasaki H (2018) Optical coherence tomography angiography to quantify choroidal neovascularization in response to Aflibercept. *Ophthalmologica* 240: 90 – 98

 © 2021 The Authors

Tan VP, Miyamoto S (2016) Nutrient-sensing mTORC1: integration of metabolic and autophagic signals. *J Mol Cell Cardiol* 95: 31 – 41

Tardito S, Oudin A, Ahmed SU, Fack F, Keunen O, Zheng L, Miletic H, Sakariassen PØ, Weinstock A, Wagner A *et al* (2015) Glutamine synthetase activity fuels nucleotide biosynthesis and supports growth of glutamine-restricted glioblastoma. *Nat Cell Biol* 17: 1556 – 1568

Wang X, Liu R, Qu X, Yu H, Chu H, Zhang Y, Zhu W, Wu X, Gao H, Tao B *et al* (2019) alpha-ketoglutarate-activated NF-kappaB signaling promotes compensatory glucose uptake and brain tumor development. *Mol Cell* 76: 148 – 162

Wang X-J, Qiao Y, Xiao MM, Wang L, Chen J, Lv W, Xu Li, Li Y, Wang Y, Tan M-D *et al* (2017) Opposing roles of acetylation and phosphorylation in LIFR-dependent self-renewal growth signaling in mouse embryonic stem cells. *Cell Rep* 18: 933 – 946

Wang X, Ye M, Wu M, Fang H, Xiao B, Xie L, Zhu X (2020) RNF213 suppresses carcinogenesis in glioblastoma by affecting MAPK/JNK signaling pathway. *Clin Transl Oncol* 22: 1506 – 1516

Ward PS, Patel J, Wise DR, Abdel-Wahab O, Bennett BD, Coller HA, Cross JR, Fantin VR, Hedvat CV, Perl AE *et al* (2010) The common feature of leukemia-associated IDH1 and IDH2 mutations is a neomorphic enzyme activity converting alpha-ketoglutarate to 2-hydroxyglutarate. *Cancer Cell* 17: 225 – 234

Xiao M, Yang H, Xu W, Ma S, Lin H, Zhu H, Liu L, Liu Y, Yang C, Xu Y *et al* (2012) Inhibition of alpha-KG-dependent histone and DNA demethylases by fumarate and succinate that are accumulated in mutations of FH and SDH tumor suppressors. *Genes Dev* 26: 1326 – 1338

Xu W, Yang H, Liu Y, Yang Y, Wang P, Kim SH, Ito S, Yang C, Wang P, Xiao MT *et al* (2011) Oncometabolite 2-hydroxyglutarate is a competitive inhibitor of alpha-ketoglutarate-dependent dioxygenases. *Cancer Cell* 19: 17 – 30

Yu G, Wang LG, Han Y, He QY (2012) clusterProfiler: an R package for comparing biological themes among gene clusters. *OMICS* 16: 284 – 287

Zengel JM, Lindahl L (1994) Diverse mechanisms for regulating ribosomal protein synthesis in Escherichia coli. *Prog Nucleic Acid Res Mol Biol* 47: 331 – 370

Zhao Q, Liu L, Xie Q (2012) In vitro protein ubiquitination assay. *Methods Mol Biol* 876: 163 – 172

© 2021 The Authors